REPORT 1152

THEORY AND PROCEDURE FOR DETERMINING LOADS AND MOTIONS IN CHINE-IMMERSED HYDRODYNAMIC IMPACTS OF PRISMATIC BODIES [1]

By Emanuel Schnitzer

SUMMARY

A theoretical method is derived for the determination of the motions and loads during chine-immersed water landings of prismatic bodies. This method makes use of a variation of two-dimensional deflected water mass over the complete range of immersion, modified by a correction for three-dimensional flow. Equations are simplified through omission of the term proportional to the acceleration of the deflected mass for use in calculation of loads on hulls having moderate and heavy beam loading. The effects of water rise at the keel are included in these equations. In order to make a direct comparison of theory with experiment, a modification of the equations was made to include the effect of finite test-carriage mass. A simple method of computation which can be applied without reading the body of this report is presented as an appendix, along with the required theoretical plots for determination of loads and motions in chine-immersed landings.

Comparisons of theory with experiment are presented as plots of impact lift coefficient and maximum draft-beam ratio against flight-path angle and as time histories of loads and motions. These comparisons cover angles of dead rise of 0° and 30°, trims up to 45°, flight-path angles up to 90°, and beam-loading coefficients from 1 to 36.5. Fair agreement is seen to exist over these ranges. The comparisons show in general that the concept involving the two-dimensional deflected mass and a three-dimensional-flow correction can be used to predict accurately the loads and motions in landings of prismatic bodies involving immersion of the chines.

INTRODUCTION

This report is concerned with the derivation of a method for calculating impact loads and motions during water landings of narrow, heavily loaded, prismatic bodies. The problem of non-chine-immersed impacts of wide, lightly loaded, prismatic hulls has been treated in reference 1. Comparisons of the theoretical results of this reference with experimental data have been made in references 1 to 4, where reasonable agreement has been demonstrated. Although these reports are devoted largely to the non-chine-immersed case, references 2 and 3 extend the theory to cover impacts during which a small amount of chine immersion is experienced.

For impacts of heavily loaded bodies involving deep immersion of the chines, reference 5 suggests that the force be determined in two main parts: (1) a part for the hull sections having nonimmersed chines, obtained by means of the theory of reference 1, and (2) a part for the hull sections having immersed chines, based on the two-dimensional separated flow about a wedge immersed in an infinite fluid (ref. 6, arts. 73 to 78). Preliminary analysis based on the equations proposed in reference 5 indicated that these equations were inadequate for the case of 0° dead-rise angle and showed some disagreement with experiment for practical immersions of narrow, heavily loaded, V-bottom bodies.

In view of the inadequacies of the procedure suggested in reference 5, a new analysis is made in the present report on the following basis: For a given transverse cross section of an immersing prismatic form, a unique relation is assumed to exist between the deflected water mass (two-dimensional) and the penetration of that section. A total deflected mass is determined by applying this variation to all cross sections along the hull, integrating over the wetted area, and applying an approximate correction to this integrated mass to account for three-dimensional flow. In the absence of a satisfactory relation for the continuous variation of two-dimensional deflected mass with draft through the region of chine immersion, relationships derived from the suggestions in reference 5 are employed. The purpose of this report is to present this new analysis and a procedure for applying it in impact calculations. Experimental verification of the theory is given.

The report is organized as follows: The differential equation of motion is derived in terms of a variation of two-dimensional deflected water mass and a correction for three-dimensional flow which is selected to satisfy the condition of steady planing. A suggested variation of this two-dimensional deflected mass with draft is given. The general solution of the equation of motion is then presented and modified by omitting the term involving acceleration of the deflected mass. A computational method is indicated for determining loads and motions in landings of prismatic bodies involving appreciable chine immersion. A further modification based on the assumption of constant forward velocity is made for comparison with experimental tank impact data. Finally, comparisons with experimental data are presented for angles of dead rise of 0° and 30°, trims from 6° to 45°, beam-loading coefficients from 1 to 36.5, and

[1] Supersedes NACA TN 2813, "Theory and Procedure for Determining Loads and Motions in Chine-Immersed Hydrodynamic Impacts of Prismatic Bodies" by Emanuel Schnitzer, 1952.

flight-path angles up to 90°. A system for determining water rise on a rectangular flat plate is given in appendix A. In appendix B a computational procedure is outlined which may be used without reading the body of the report.

SYMBOLS

(Any consistent system of units may be used)

β	Bobyleff's flow coefficient, a function of dead rise
b	beam of hull at chines
C'	ratio of water rise at keel to draft, r/z
C_L	impact lift coefficient, $\frac{(n_{i_w})_{max}W}{\frac{\rho}{2}b^2V_0^2}$
C_Δ	beam-loading coefficient, $W/\rho g b^3$
F_N	hydrodynamic force on hull normal to keel
g	acceleration due to gravity
J	parameter involving three-dimensional deflected mass
k	generalized draft parameter for free-body landing
l	wetted length along keel
m_w	two-dimensional deflected water mass in transverse plane
n_{i_w}	impact load factor measured normal to undisturbed water surface, $-\frac{\ddot{z}}{g}$
Q	velocity-reduction parameter for free-body landing
Q_L	velocity-reduction parameter for landings involving horizontal constraint
r	water rise at keel normal to undisturbed water surface
$\dot{r}$	vertical velocity of water rise at keel
s	distance from foremost immersed station along keel to flow plane
$\dot{s}$	velocity of flow plane relative to float in direction parallel to keel
$\ddot{s}$	acceleration of flow plane relative to float in direction parallel to keel
t	time after water contact
V	resultant velocity of hull
W	weight of airplane
$\dot{x}$	horizontal velocity of float
z	immersion of keel at step normal to undisturbed water surface, positive down
$\dot{z}$	vertical velocity of float
$\ddot{z}$	vertical acceleration of float
β	angle of dead rise, radians
$f(\beta)$	dead-rise function
γ	flight-path angle relative to undisturbed water surface
ζ	immersion of keel below undisturbed water surface, normal to itself into a flow plane, positive downward
$\dot{\zeta}$	velocity of float normal to keel, $\dot{x}\sin\tau+\dot{z}\cos\tau$
$\ddot{\zeta}$	acceleration of float normal to keel
ζ'	immersion of the keel normal to itself into a flow plane, corrected for water rise at keel
$\dot{\zeta}'$	partial derivative of ζ' with respect to time
κ	approach parameter for free-body landing, $\frac{\sin\tau}{\sin\gamma_0}\cos(\tau+\gamma_0)$
κ_L	approach parameter for landings involving horizontal constraint, $\tan\tau/\tan\gamma_0$
λ	ratio of length of keel below undisturbed water surface to mean beam
λ'	ratio of length of keel below elevated water surface to mean beam
ρ	mass density of water
σ	hull cross-sectional-shape factor
τ	trim (between keel and undisturbed water surface)
$\varphi(\lambda')$	Pabst's aspect-ratio correction based on λ'.
$\varphi\left(\frac{1}{\lambda}\right)$	Pabst's aspect-ratio correction based on $1/\lambda$

Subscripts:

c	at chine immersion
max	maximum
0	at water contact
s	at step

THEORY FOR PRISMATIC CHINE-IMMERSED IMPACT

EQUATION OF MOTION

This derivation for the motion of a long, narrow body landing on a smooth water surface (fig. 1) is based on the concept that the flow occurs primarily in transverse planes which are fixed in space and oriented normal to the keel (refs. 1 to 5). Thus, a two-dimensional treatment with a three-dimensional-flow or aspect-ratio correction factor is made, as is usual in the calculation of the dynamics of such bodies. The effects of buoyancy, viscosity, and changes in trim are believed to be very small for practical impacts and are neglected. As in references 1 to 5, therefore, the reaction in a given flow plane of length ds (fig. 1) is defined in terms of the momentum of the fluid as

$$dF_N=\frac{\partial}{\partial t}(m_w\dot{\zeta})\,ds \tag{1}$$

where $m_w\,ds$ is an equivalent deflected mass of fluid and $\dot{\zeta}$ is the normal velocity of the body. The total hydrodynamic force on the body is then obtained by integrating equation (1) over the wetted surface and applying the correction for three-dimensional flow $\varphi(\lambda')$ (hereinafter designated three-dimensional correction):

$$F_N=\varphi(\lambda')\int_0^l\frac{\partial}{\partial t}(m_w\dot{\zeta})\,ds \tag{2}$$

Assuming that external forces, such as the wing lift force in the case of seaplanes, are equal and opposite to the weight and applying Newton's second law to equation (2) as in references 1 to 5 leads to the following differential equation for the motion normal to the keel during impact:

$$-\frac{W}{g}\ddot{\zeta}=\varphi(\lambda')\left(\int_0^l\dot{\zeta}\frac{\partial m_w}{\partial t}\,ds+\ddot{\zeta}\int_0^l m_w\,ds\right) \tag{3}$$

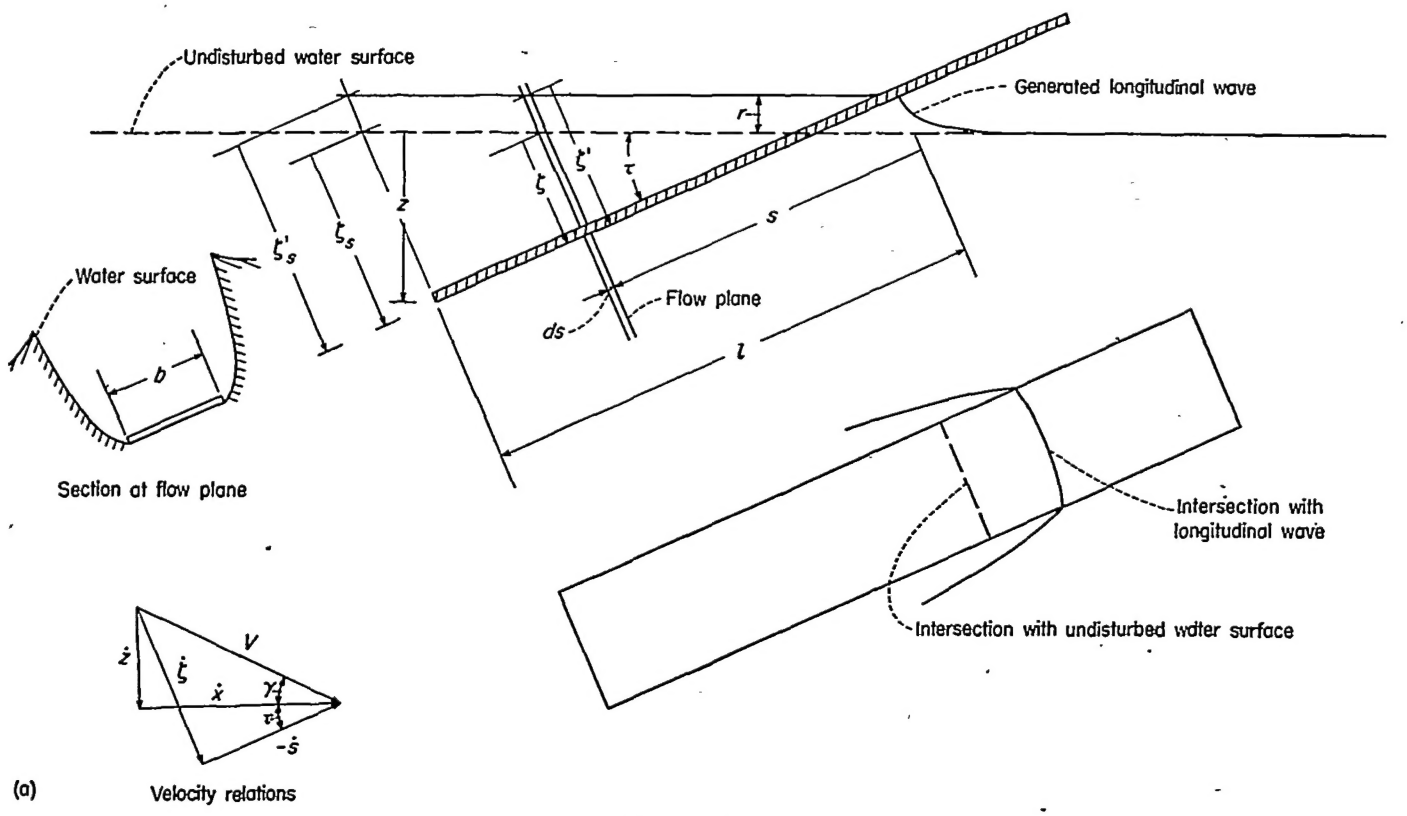

(a) Flat plate.

FIGURE 1.—Geometric relations during impact.

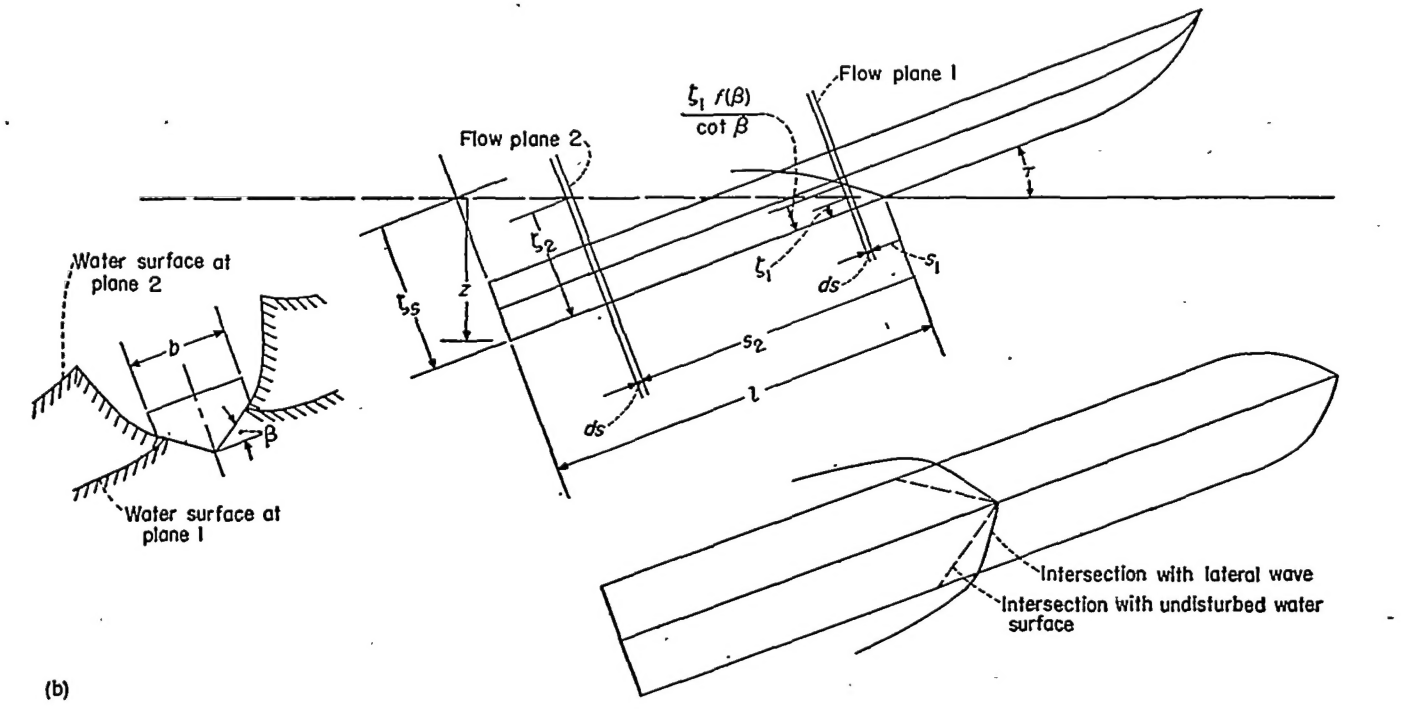

(b) Body with dead rise

FIGURE 1.—Concluded.

This basic equation of motion can be solved specifically, provided that m_w and $\varphi(\lambda')$ are known. Although this equation may not hold for accelerated motion at very large (infinite) immersions, it is believed to apply over the practical range of impacts.

SELECTION OF THREE-DIMENSIONAL DEFLECTED MASS

The three-dimensional-flow correction $\varphi(\lambda')$ and the two-dimensional deflected mass m_w will be defined and evaluated before the procedure for solving equation (3) is presented.

Determination of three-dimensional correction.—The three-dimensional-flow correction to be used in this report was determined empirically by Pabst in reference 7 and is given by the quation

$$\varphi(\lambda')=\left[\frac{1}{1+\frac{1}{(\lambda')^2}}\right]^{1/2}\left(1-\frac{0.425}{\lambda'+\frac{1}{\lambda'}}\right) \tag{4}$$

which is plotted in figure 2. The value λ' is taken as the ratio of the length of keel below the elevated water surface to the mean wetted width (see fig. 1). The hydrodynamic aspect ratio λ' for a rectangular flat plate is therefore expressed by the equation

$$\lambda'=\frac{l}{b} \tag{5}$$

where l is the length of keel below the elevated water surface and b is the beam of the body at the chines.

For a V-bottom prismatic body the water rise at the keel is neglected so that $\lambda'=\lambda$ and $\zeta'_s=\zeta_s$ (see fig. 1). The "lateral" water rise as shown in figure 1(b) at flow plane 1 and discussed in reference 2 is, however, taken into account in determining the mean wetted width. On this basis, the ratio of the wetted keel length to the mean wetted width is found to be

$$\lambda=\frac{1}{\tan\tau\, f(\beta)} \qquad \left(\frac{\zeta_s}{b}\leqq\frac{\tan\beta}{2}\right) \tag{6}$$

or

$$\lambda=\frac{(\zeta_s/b)^2}{\tan\tau\left[\frac{\zeta_s}{b}-\frac{1}{4f(\beta)}\right]} \qquad \left(\frac{\zeta_s}{b}>\frac{\tan\beta}{2}\right) \tag{7}$$

where

$$f(\beta)=\frac{\pi}{2\beta}-1 \tag{8}$$

and β is the angle of dead rise.

A certain measure of the suitability of equations (4) to (8) can be obtained by considering the case of steady planing. For this case ($\ddot{\zeta}=0$), equation (2) reduces to

$$F_N=\varphi(\lambda')\dot{\zeta}\int_0^l\frac{\partial m_w}{\partial t}\,ds \tag{9}$$

In order to consider this equation further, the assumption is made that the two-dimensional-deflected-mass ratio defined as $m_w/\rho b^2$ is a function of only the cross-sectional shape of the body and the ratio of normal draft to beam; that is,

$$\frac{m_w}{\rho b^2}=f\left(\sigma,\frac{\zeta'}{b}\right) \tag{10}$$

where ρ is the mass density of the fluid and σ is the cross-sectional-shape factor. On the basis of this assumption and the substitution $ds=d(\zeta\cot\tau)=d(\zeta'\cot\tau)$ (see fig. 1), equation (9) may be written

$$\begin{aligned}F_N&=\varphi(\lambda')\dot{\zeta}\int_0^{\zeta'_s}\frac{dm_w}{d\zeta'}\frac{\partial\zeta'}{\partial t}\,d(\zeta'\cot\tau)\\&=\frac{\varphi(\lambda')\dot{\zeta}}{\tan\tau}\int_0^{\zeta'_s}\frac{dm_w}{d\zeta'}\frac{\partial\zeta}{\partial t}\,d\zeta'\\&=\frac{\varphi(\lambda')\dot{\zeta}^2}{\tan\tau}\int_0^{m_{w_s}}dm_w\\F_N&=\frac{\varphi(\lambda')\dot{\zeta}^2m_{w_s}}{\tan\tau}\end{aligned} \tag{11}$$

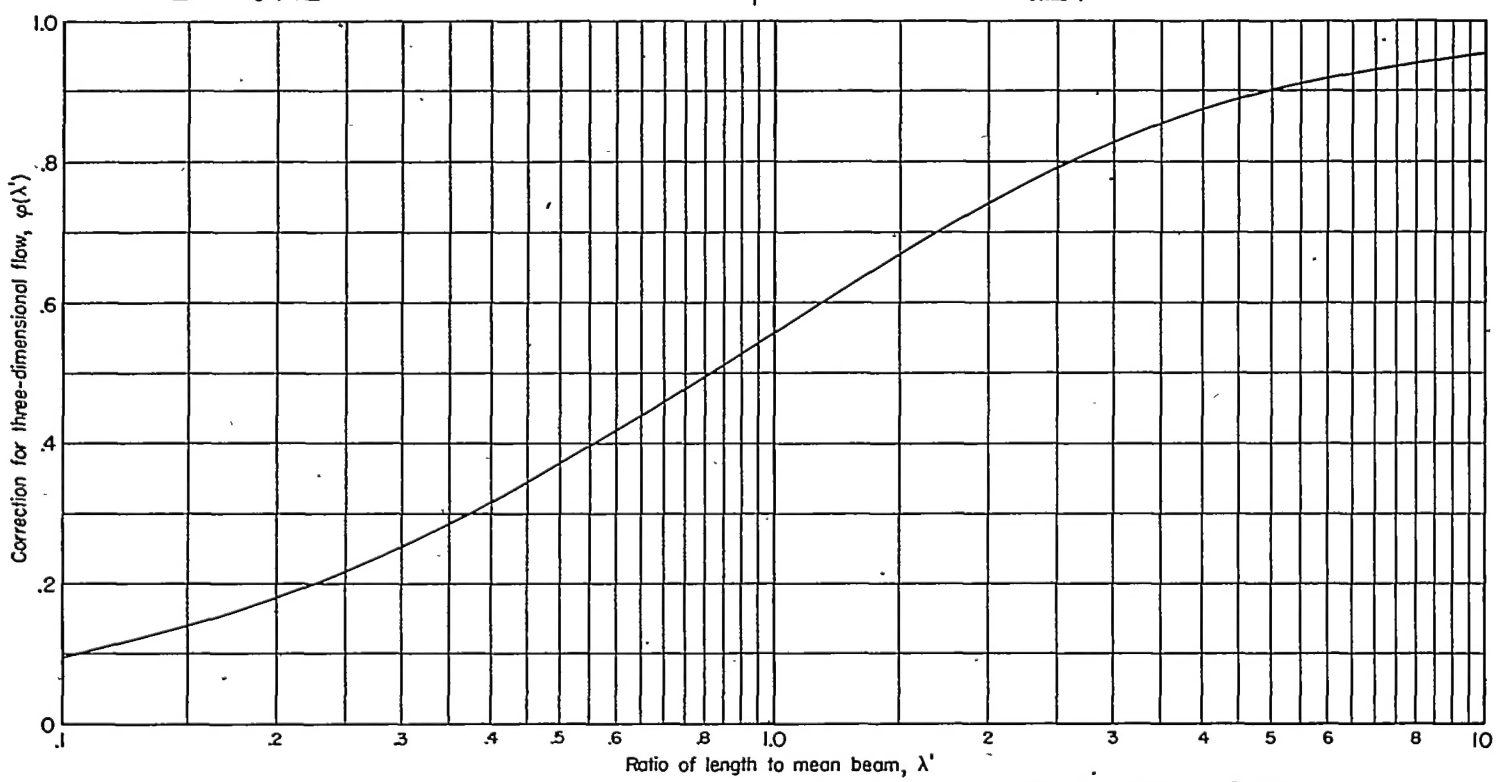

FIGURE 2.—Pabst's correction factor for three-dimensional flow (ref. 7). $\varphi(\lambda')=\left[\frac{1}{1+\frac{1}{(\lambda')^2}}\right]^{1/2}\left(1-\frac{0.425}{\lambda'+\frac{1}{\lambda'}}\right)$.

where m_{w_s} is the two-dimensional deflected water mass which in seaplanes is associated with the flow plane at the step. Solution of equation (11) for m_{w_s} and division through by ρb^2 to render the equation nondimensional gives

$$\frac{m_{w_s}}{\rho b^2}=\frac{F_N \tan \tau}{\varphi(\lambda')\dot{\zeta}^2 \rho b^2} \tag{12}$$

In order to investigate this equation, use has been made of high-speed, experimental planing data (refs. 8 and 9) obtained at the Langley tank no. 1 with prismatic forms having angles of dead rise of 0° to 40°. When the right-hand side of equation (4) is substituted for $\varphi(\lambda')$ and the experimental data of references 8 and 9 are substituted into equation (12), the factor $m_{w_s}/\rho b^2$ is found to be essentially a function of only the angle of dead rise β and the ratio of normal draft at the step to beam ζ'_s/b, or

$$\frac{m_{w_s}}{\rho b^2}=f\left(\beta, \frac{\zeta'_s}{b}\right) \tag{13}$$

This result substantiates the assumptions of equation (10) and also demonstrates the validity of the three-dimensional correction expressed by equations (4) to (8), for the case of the V-bottom prism.

Two-dimensional deflected mass.—In the absence of a theory covering the continuous variation of two-dimensional deflected mass with draft over the complete range of immersion, the two separate variations suggested in reference 5 are combined in this report to give a single mass variation with draft. This variation is selected as follows:

(1) Sections prior to chine immersion:

For non-chine-immersed sections the deflected mass is generally taken as the virtual mass, which is defined herein as the apparent additional mass observed during accelerated motion. In references 10 and 11 theories are available for determining the variation of virtual mass with draft for non-chine-immersed impacts. These theories have been checked experimentally for the prismatic V-bottom form and that of reference 10 was checked also for the scalloped-bottom form. For cross sections of arbitrary shape, the variation of the two-dimensional deflected mass may be obtained from reference 3, 10, or 12. However, experience has shown that, for small transverse concave curvature, the mass variation may be approximated by an average V-shape. The same approximation is believed to be equally valid for small convex curvatures. The two-dimensional-mass variation for a V-shape is

$$m_w=\frac{\rho \pi \zeta^2}{2}[f(\beta)]^2 \tag{14}$$

which is taken from references 1 to 3 and is based on Wagner's work. Substitution of ζ' for ζ in this equation to take water rise at the keel into account gives

$$m_w=\frac{\rho \pi (\zeta')^2}{2}[f(\beta)]^2 \tag{15}$$

which is to be used as the deflected mass prior to chine immersion of each section. Chine immersion is herein assumed to occur at the intersection of the chines in a given flow plane with a plane parallel to the undisturbed water surface and passing through the intersection point of the keel with the actual water surface. The draft-beam ratio at chine immersion is

$$\frac{\zeta'_c}{b}=\frac{\tan \beta}{2} \tag{16}$$

The two-dimensional deflected mass at this instant therefore becomes

$$m_w=\frac{\rho \pi b^2}{8}[f(\beta)]^2 \tan^2 \beta \tag{17}$$

(2) Sections subsequent to chine immersion:

For infinite immersion of the chines, a variation of two-dimensional deflected mass with draft may be derived from the theory of Bobyleff (ref. 6, arts. 73 to 78). However, no theory is believed to be available on the variation of two-dimensional deflected mass for moderate chine immersion. In the absence of a single accurate deflected-mass variation over the entire range of immersion, a composite deflected mass is suggested which is composed of the deflected mass present at the instant of chine immersion plus a deflected mass which is derived from Bobyleff's theory. For infinite immersions, Bobyleff has shown that the force per unit length on a two-dimensional V-shape of finite width b traveling with constant normal velocity $\dot{\zeta}'$ (point foremost) is

$$F_N=B\frac{\rho}{2}(\dot{\zeta}')^2 b \tag{18}$$

where B is a function of the angle of dead rise and is given in figure 3. This force is assumed to be equal to the rate of change of momentum of an equivalent deflected mass; that is,

$$\begin{aligned} F_N&=\frac{d}{dt}(m_w \dot{\zeta}') \\ &=(\dot{\zeta}')^2 \frac{dm_w}{d\zeta'} \end{aligned} \tag{19}$$

where constant velocity is assumed. Thus, from equations (18) and (19),

$$\frac{dm_w}{d\zeta'}=B\frac{\rho}{2}b \tag{20}$$

which in this report is taken as the variation of deflected mass with draft subsequent to chine immersion. Integrating to find the change in deflected mass subsequent to chine immersion Δm_w gives

$$\begin{aligned} \Delta m_w&=B\frac{\rho}{2}b\int_{\zeta'_c}^{\zeta'} d\zeta' \\ &=B\frac{\rho}{2}b(\zeta'-\zeta'_c) \end{aligned} \tag{21}$$

The total two-dimensional deflected mass subsequent to chine immersion is found by adding to this expression the deflected mass at the instant of chine immersion. If this latter mass is assumed to be given by equation (17), the total mass becomes

$$m_w=\frac{\rho \pi b^2}{8}[f(\beta)\tan \beta]^2+B\frac{\rho}{2}b^2\left(\frac{\zeta'}{b}-\frac{\tan \beta}{2}\right) \tag{22}$$

For prismatic hulls of arbitrary cross-sectional shape where the variation from a V-section is not great, approximate values of m_w are believed to be obtainable through substitution of equivalent V-sections for the arbitrary sections. The

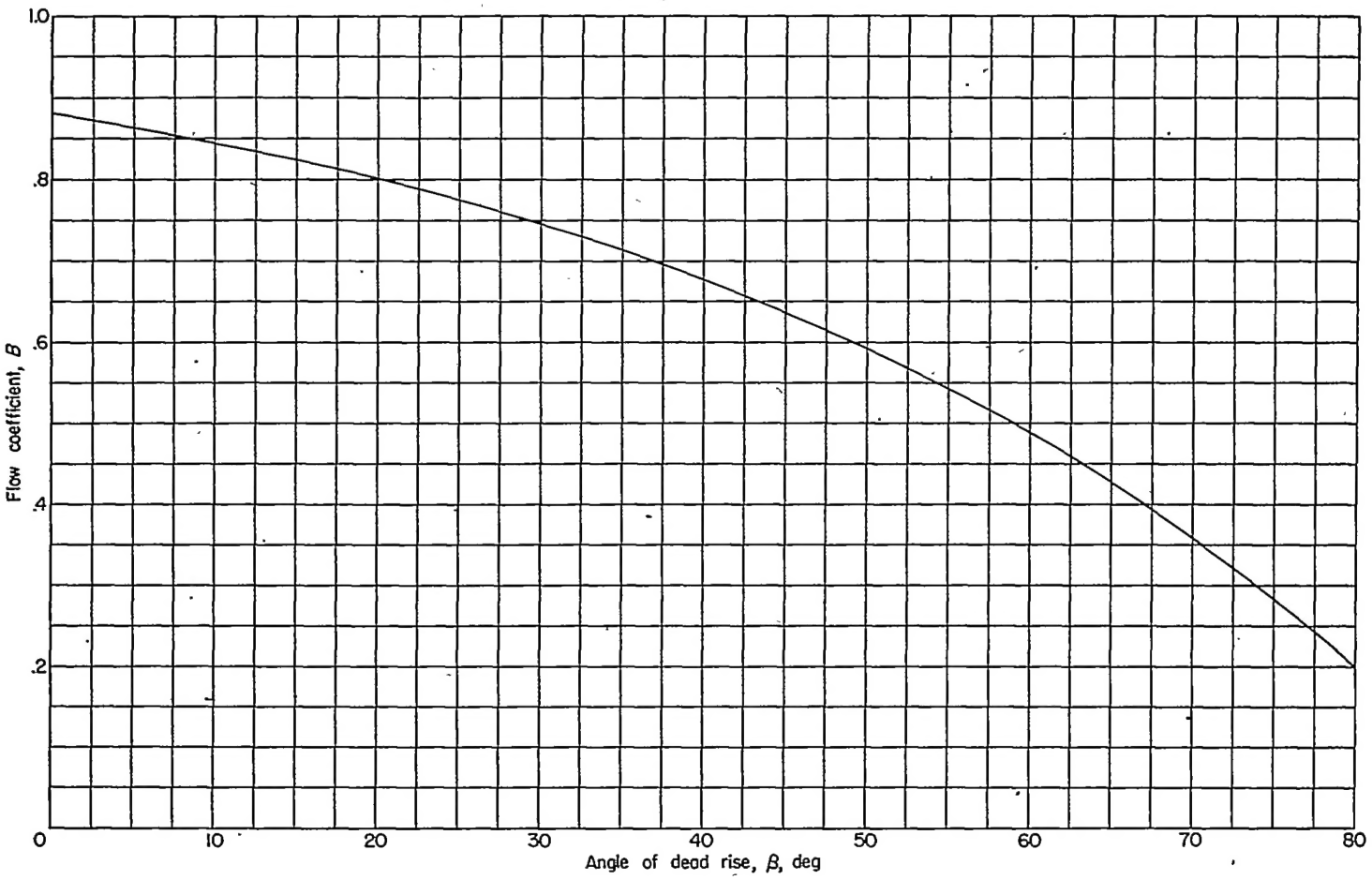

FIGURE 3.—Variation of flow coefficient with angle of dead rise (ref. 6, arts. 73 to 78).

angle of dead rise would be determined by obtaining an average angle of dead rise for the arbitrary section.

For the case of 0° dead-rise angle, equation (22) reduces to

$$m_w=\rho b^2\left(\frac{\pi^3}{32}+0.44\,\frac{\zeta'}{b}\right) \tag{23}$$

Equations (15), (22), and (23) are to be used in the solution of equation (3).

METHOD FOR SOLVING EQUATION OF MOTION INCLUDING COMPUTATIONAL CHARTS

GENERAL TREATMENT

The incorporation of the aspect-ratio correction $\varphi(\lambda')$ and the deflected mass m_w into equation (3) permits solution of the equation by numerical methods. A large saving of time may be effected, however, by solving the equation partially by analytical means to reduce it to a form convenient for graphical integration. This reduction is given here, with equation (3) restated first for convenience:

$$-\frac{W}{g}\ddot{\zeta}=\varphi(\lambda')\left(\int_0^l \dot{\zeta}\,\frac{\partial m_w}{\partial t}\,ds+\ddot{\zeta}\int_0^l m_w\,ds\right)$$

The discussion following equation (10) substantiates the assumption expressed by that equation that the two-dimensional deflected mass for a given hull is a function only of the draft normal to the keel; that is,

$$m_w=f(\zeta') \tag{24}$$

Therefore,

$$\frac{\partial m_w}{\partial t}=\frac{\partial m_w}{\partial \zeta'}\frac{\partial \zeta'}{\partial t}=\frac{dm_w}{d\zeta'}\dot{\zeta}' \tag{25}$$

From figure 1, $s=\dfrac{\zeta'}{\tan\tau}$. Differentiating this relation gives

$$ds=\frac{d\zeta'}{\tan\tau} \tag{26}$$

Substitution of equations (25) and (26) into equation (3) gives

$$-\frac{W}{g}\ddot{\zeta}=\varphi(\lambda')\left(\int_0^{m_{w_s}}\frac{\dot{\zeta}\dot{\zeta}'}{\tan\tau}\,dm_w+\ddot{\zeta}\int_0^l m_w\,ds\right) \tag{27}$$

For impacts with deeply immersed chines, however, the water rise at the keel r (see fig. 1) is generally small compared with the draft and is approximately constant for the

greater drafts. Therefore, its derivative with respect to time $\dot{r}$ approaches zero at these drafts, making $\dot{\zeta}'$, which is equal to $\dot{\zeta}+\dot{r}\sec\tau$, approach $\dot{\zeta}$. In this derivation, then, $\dot{\zeta}'$ is assumed equal to $\dot{\zeta}$, whereby

$$-\frac{W}{g}\ddot{\zeta}=\varphi(\lambda')\left(\frac{\dot{\zeta}^2}{\tan\tau}\int_0^{m_{w_s}}dm_w+\ddot{\zeta}\int_0^l m_w\,ds\right) \tag{28}$$

and, after integration of the first term on the right-hand side,

$$\ddot{\zeta}\left[1+\frac{g}{W}\varphi(\lambda')\int_0^l m_w\,ds\right]=-\frac{\dot{\zeta}^2\varphi(\lambda')gm_{w_s}}{W\tan\tau} \tag{29}$$

Rewriting equation (29) in terms of the coordinate system referred to the water surface is done by means of the following substitutions (see fig. 1):

$$\ddot{\zeta}=\frac{\ddot{z}}{\cos\tau} \tag{30a}$$

$$\dot{\zeta}=\frac{\dot{z}}{\cos\tau}-\dot{s}\tan\tau \tag{30b}$$

$$\zeta_s=\frac{z}{\cos\tau} \tag{30c}$$

where $\ddot{s}$ is taken equal to 0 because of the assumption of frictionless flow and no external force, and $\dot{s}$ is therefore a constant. When these substitutions are made, equation (29) becomes

$$\ddot{z}\left[1+\frac{g\varphi(\lambda')}{W}\int_0^l m_w\,ds\right]=-(\dot{z}-\dot{s}\sin\tau)^2\frac{g\varphi(\lambda')m_{w_s}}{W\sin\tau} \tag{31}$$

Rearranging the terms and integrating both sides with respect to z gives

$$\int_0^z\frac{\ddot{z}\,dz}{(\dot{z}-\dot{s}\sin\tau)^2}=-\int_0^z\frac{\frac{m_{w_s}}{\sin\tau}dz}{\frac{W}{g\varphi(\lambda')}+\int_0^l m_w\,ds} \tag{32}$$

which can be written

$$\int_{\dot{z}_0}^{\dot{z}}\frac{\dot{z}\,d\dot{z}}{(\dot{z}-\dot{s}\sin\tau)^2}=-\int_0^z\frac{\frac{m_{w_s}}{\sin\tau}dz}{\frac{W}{g\varphi(\lambda')}+\int_0^l m_w\,ds} \tag{33}$$

After the integration of the left-hand side has been performed, the following equation expressing the velocity as a function of the draft is obtained:

$$\log_e\frac{\frac{\dot{z}}{\dot{z}_0}+\kappa}{1+\kappa}+\frac{\kappa}{\frac{\dot{z}}{\dot{z}_0}+\kappa}-\frac{\kappa}{1+\kappa}=-\int_0^z\frac{\frac{m_{w_s}}{\sin\tau}dz}{\frac{W}{g\varphi(\lambda')}+\int_0^l m_w\,ds} \tag{34}$$

where

$$\kappa=-\frac{\dot{s}\sin\tau}{\dot{z}_0}$$

$$=\frac{\sin\tau}{\sin\gamma_0}\cos(\tau+\gamma_0)$$

If for convenience the left-hand side of equation (34) is denoted by $Q\left(\frac{\dot{z}}{\dot{z}_0},\kappa\right)$, and if dz as obtained by differentiating equation (30c) is substituted into the right-hand side, the following equation results:

$$Q=-\int_0^{\zeta_s}\frac{\frac{m_{w_s}d\zeta_s}{\tan\tau}}{\frac{W}{g\varphi(\lambda')}+\int_0^l m_w\,ds} \tag{35}$$

Since, from equation (24), $m_{w_s}=f(\zeta'_s)$, a multiplication by $d\zeta'_s/d\zeta'_s$ is performed inside the integral to give

$$Q=-\int_0^{\zeta'_s}\frac{\frac{m_{w_s}}{\tan\tau}\frac{d\zeta_s}{d\zeta'_s}d\zeta'_s}{\frac{W}{g\varphi(\lambda')}+\int_0^l m_w\,ds} \tag{36}$$

Equation (36) can be expressed in terms of nondimensional quantities through multiplication of the right-hand side by $\rho b^3/\rho b^3$; after substitution of equation (26), the following relation results:

$$Q=-\int_0^{\zeta'_s/b}\frac{\frac{m_{w_s}}{\rho b^2}\frac{d\zeta_s}{d\zeta'_s}d\frac{\zeta'_s}{b}}{\frac{C_\Delta\tan\tau}{\varphi(\lambda')}+\int_0^{\zeta'_s/b}\frac{m_{w_s}}{\rho b^2}d\frac{\zeta'_s}{b}} \tag{37}$$

where

$$C_\Delta=\frac{W}{\rho g b^3}$$

Since Q, which denotes the left-hand side of equation (34), contains the velocity ratio $\dot{z}/\dot{z}_0$, equation (37) represents, finally, the relation between this velocity ratio and the ratio of normal draft to beam ζ'_s/b.

The relation between the nondimensional acceleration $\ddot{z}b/\dot{z}_0^2$ and the nondimensional vertical-velocity and draft-beam ratios is determined through similar nondimensionalizing of equation (31), which results in the equation

$$\frac{\ddot{z}b}{\dot{z}_0^2}=-\frac{\left(\frac{\dot{z}}{\dot{z}_0}+\kappa\right)^2\frac{1}{\cos\tau}\frac{m_{w_s}}{\rho b^2}}{\frac{C_\Delta\tan\tau}{\varphi(\lambda')}+\int_0^{\zeta'_s/b}\frac{m_{w_s}}{\rho b^2}d\frac{\zeta'_s}{b}} \tag{38}$$

Equations (37) and (38) can be used to calculate the variation of acceleration and velocity with draft during

fixed-trim impacts involving appreciable chine immersion. In order to effect specific solutions of these equations, the variables making up the equations are presented in the form of computational charts, some of which are described in the next paragraph. An indicated method of computation follows.

The variation of κ with γ_0 is given in figure 4 for various trim angles. The left-hand side of equation (34), designated as Q in equation (37), is plotted against κ for various values of $\dot{z}/\dot{z}_0$ in figure 5. The ratio $d\zeta_s/d\zeta'_s$ in equation (37) is the keel water-rise factor which in reference 13 was shown to be substantially independent of flight-path angle and therefore capable of being evaluated from planing data. For the rectangular flat plate, a large quantity of experimental planing data is available from which this factor can be computed. An analysis based on these planing data and giving the wetted length and the keel water-rise factor $\frac{d\zeta_s}{d\zeta'_s}=\frac{d\lambda}{d\lambda'}$ for landings of flat plates is presented in appendix A and the results are plotted in figure 6. For the case of finite dead rise this factor has not been fully evaluated, but since it is believed to be close to unity (no water rise), it is assigned that value in this report for angles of dead rise greater than 10°. For angles of dead rise smaller than 10°, use of the keel water-rise factor $d\zeta_s/d\zeta'_s$ for the flat plate is suggested.

In order to obtain specific solutions of equations (37) and (38) in the forms shown for flat or V-bottom prismatic bodies, the following procedure is suggested: The variation of m_{w_s} with ζ'_s may be obtained from equations (15) and (22) and figure 3, from equation (23) and figure 3, or from experimental planing data with the aid of equation (12). This mass variation may be substituted into the integral in the denominator of equations (37) and (38) and integrated analytically or graphically. The aspect ratio λ' may be determined from equations (5) to (8) as a function of the ratio of normal draft to beam (λ' is taken equal to λ for a hull with dead rise). For a flat plate, l in equation (5) is related to the normal draft (see fig. 1) by the equation $l=\frac{\zeta'_s}{\tan\tau}$. The variation of $\varphi(\lambda')$ with λ' may then be obtained from figure 2. The variation of $d\zeta_s/d\zeta'_s$ may be obtained from figure 6 (b) for angles of dead rise smaller than 10° and is taken as unity for angles of dead rise of 10° and greater. After these quantities have been substituted into equation (37), it can be integrated graphically to yield the variation of Q with ζ'_s/b. The variation of $\dot{z}/\dot{z}_0$ with Q may be obtained from figure 5 after selecting a value of κ from figure 4; thus, the variation of $\dot{z}/\dot{z}_0$ with ζ'_s/b may be established. A value of $\ddot{z}b/\dot{z}_0^2$ can then be obtained for each value of $\dot{z}/\dot{z}_0$ through substitution of the derived quantities into equation (38).

The ratio of vertical draft to beam can be found from the ratio of normal draft to beam by means of the equation

$$\frac{z}{b}=\frac{\zeta'_s}{b}\frac{\zeta_s}{\zeta'_s}\cos\tau \tag{39}$$

where ζ_s/ζ'_s is assumed to be equal to λ/λ', which may be obtained from figure 6 (a) for angles of dead rise smaller than 10° and is taken as unity for angles of dead rise of 10° and greater. For the case of 0° dead rise, equation (39) can also be written

$$\frac{z}{b}=\lambda'\frac{\lambda}{\lambda'}\sin\tau \tag{40}$$

The variations of acceleration and velocity with draft as obtained by use of equations (37) to (40) allow design maximums to be established. For calculating structural response, time histories are desirable. From the relations $dz=\dot{z}\,dt$, $d\dot{z}=\ddot{z}\,dt$, and $\dot{z}_0=V_0\sin\gamma_0$ a time coefficient may be derived which is defined by either of the following equations:

$$\left.\begin{aligned}\frac{tV_0}{b}&=\frac{1}{\sin\gamma_0}\int_0^{z/b}\frac{d\frac{z}{b}}{\frac{\dot{z}}{\dot{z}_0}}\\ \frac{tV_0}{b}&=\frac{1}{\sin\gamma_0}\int_1^{\dot{z}/\dot{z}_0}\frac{d\frac{\dot{z}}{\dot{z}_0}}{\frac{\ddot{z}b}{\dot{z}_0^2}}\end{aligned}\right\} \tag{41}$$

where V_0 is the initial resultant velocity at contact. Graphical integration of either of these equations allows the draft-time relation to be established. It should be noted that the integrand of the first equation becomes infinite for $\frac{\dot{z}}{\dot{z}_0}=0$ (maximum draft), whereas the integrand of the second equation becomes infinite for $\frac{\ddot{z}b}{\dot{z}_0^2}=0$ (water contact and water exit). It is, therefore, expedient in obtaining the time variation to make use of both equations in the following manner. The time increment from water contact to some draft less than the maximum is obtained from the first equation. The time increment including the maximum draft is obtained from the second equation, and the final time increment to water exit is obtained from the first equation. Appropriate limits of integration must of course be substituted for those given in these equations.

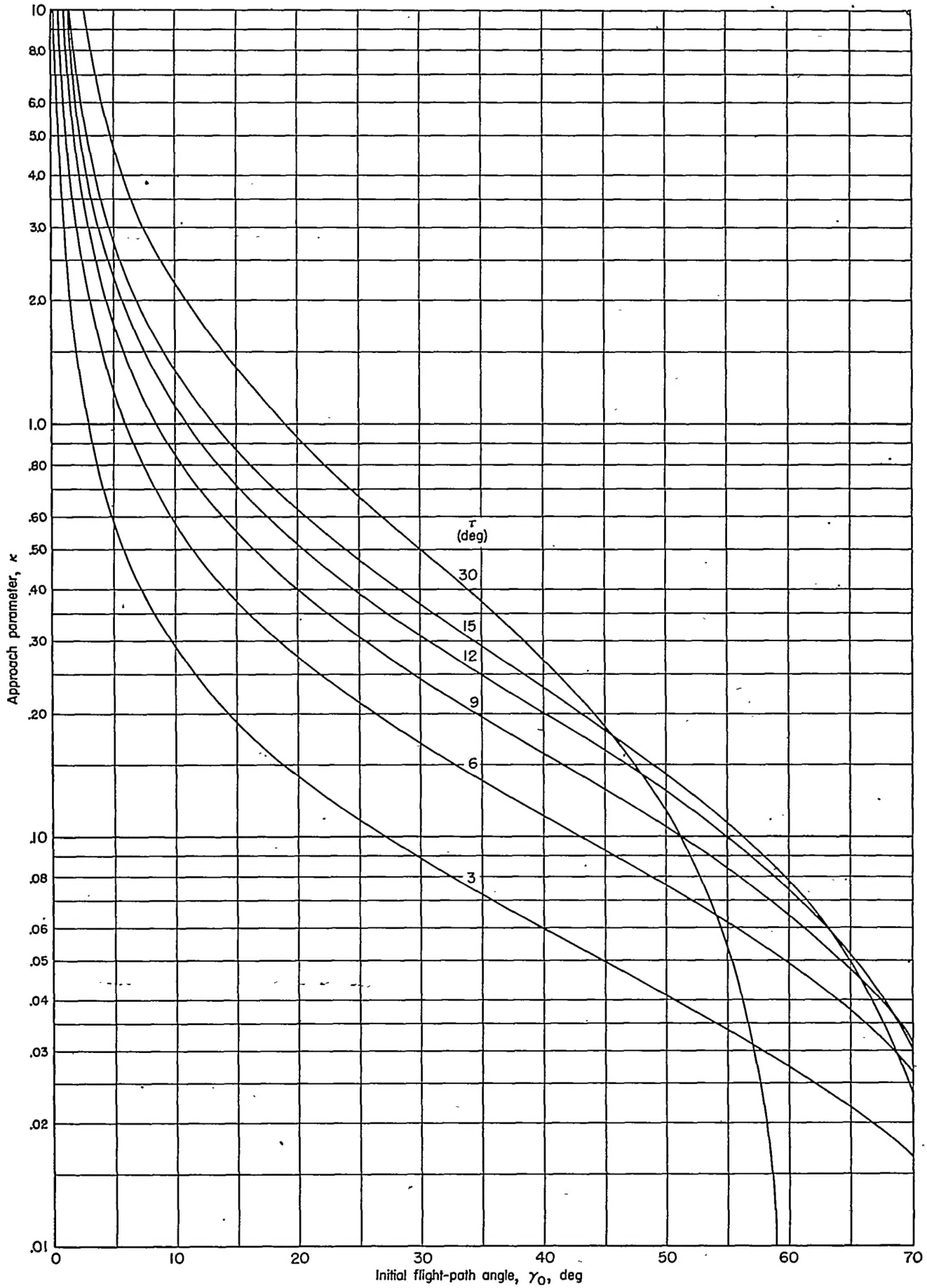

FIGURE 4.—Variation of approach parameter with trim and flight-path angle. $\kappa=\frac{\sin \tau}{\sin \gamma_0} \cos (\tau+\gamma_0)$.

321605—55——65

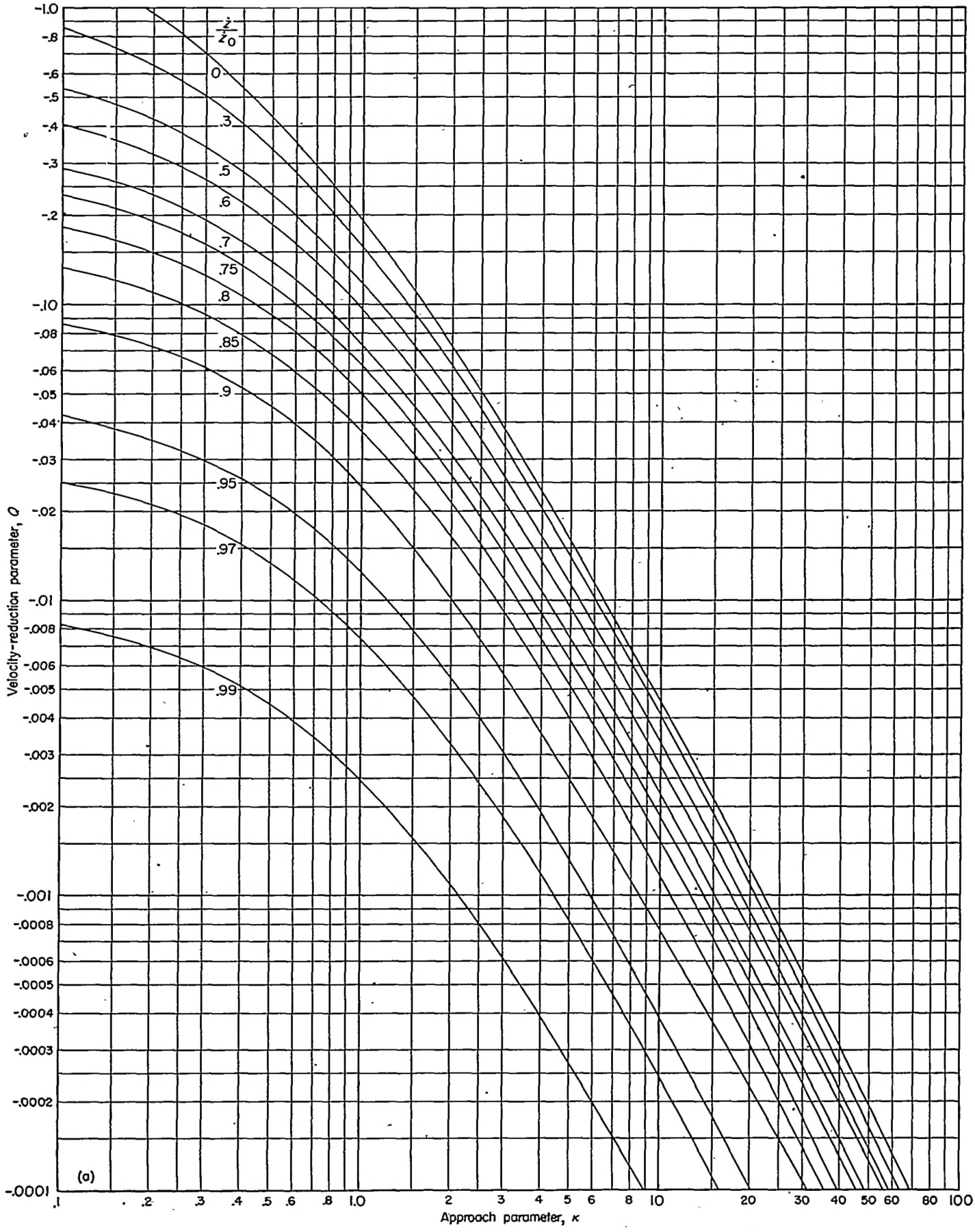

(a) Penetration.

FIGURE 5.—Variation of velocity reduction parameter for various velocity ratios. $Q=\log_e \frac{\frac{\dot{z}}{\dot{z}_0}+\kappa}{1+\kappa}+\frac{\kappa}{\frac{\dot{z}}{\dot{z}_0}+\kappa}-\frac{\kappa}{1+\kappa}$

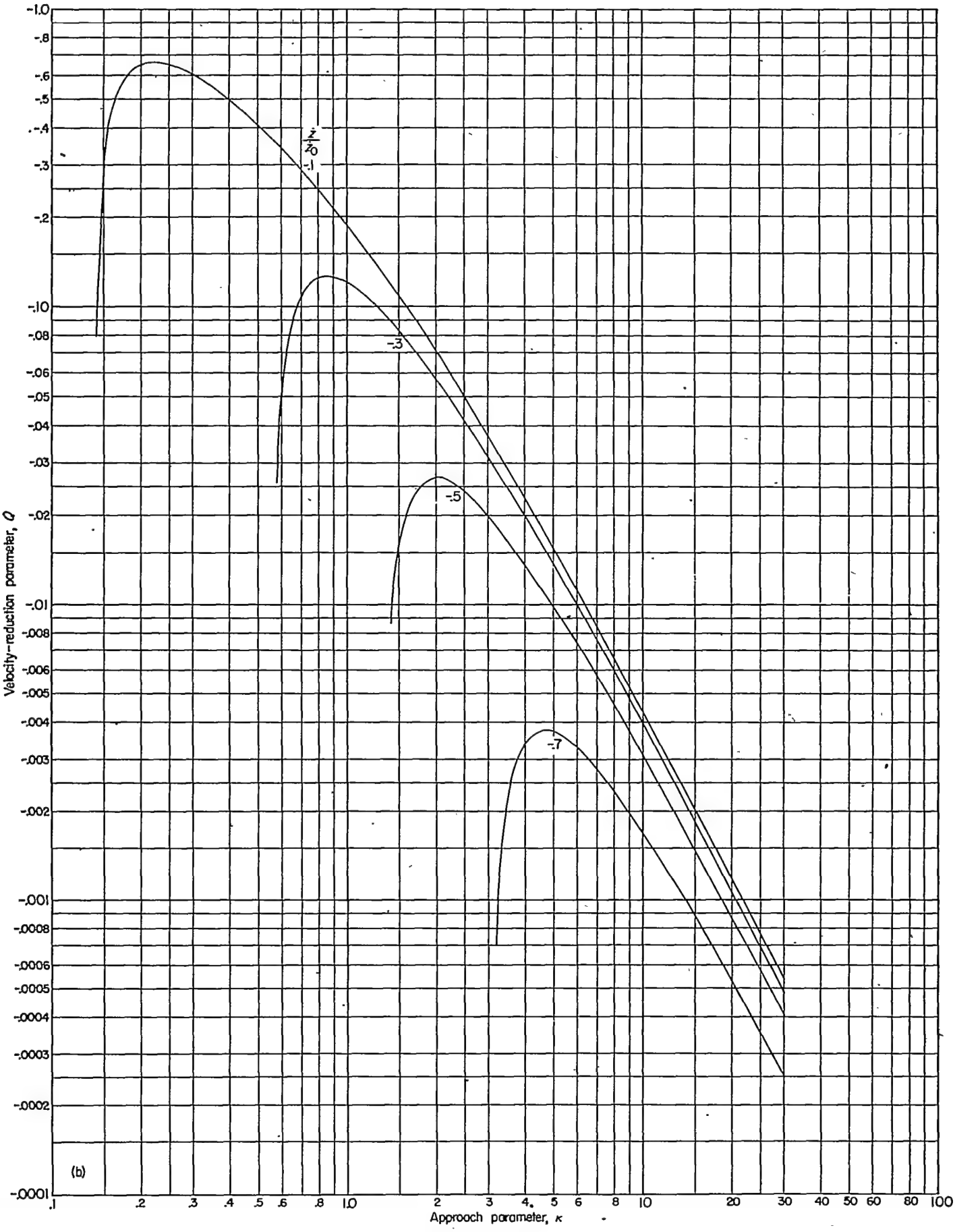

(b) Rebound.

FIGURE 5.—Concluded

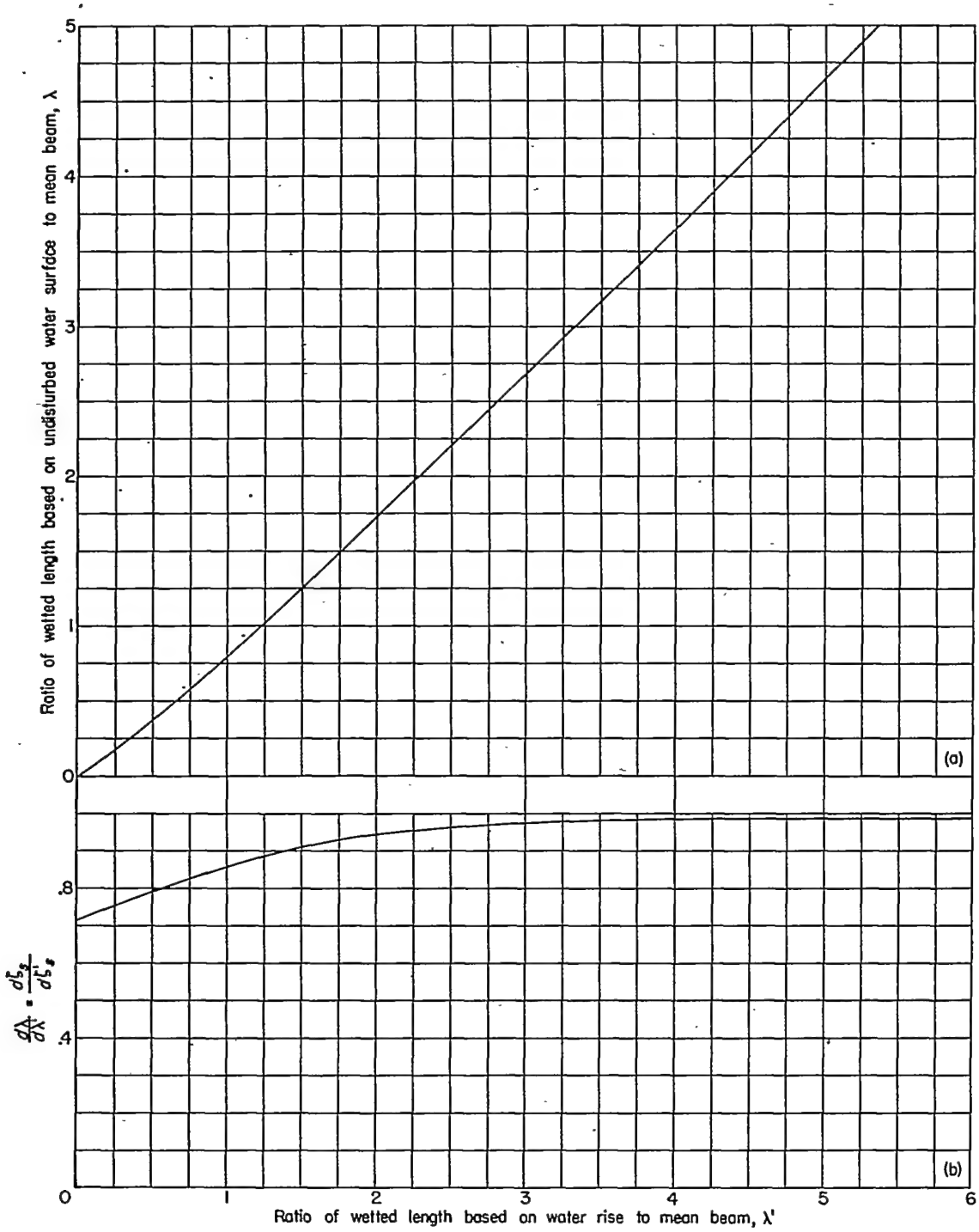

(a) Wetted-length variations.

(b) Variation of derivative of wetted length ratio with ratio of wetted length based on water rise to mean beam.

FIGURE 6.—Water-rise variations for a flat plate.

[SIMPLIFICATION THROUGH OMISSION OF ACCELERATION TERM

In order to reduce the labor required to make solutions for specific landing impacts, a simplification was effected which does not seriously reduce the accuracy of these solutions for practical landing configurations. From equation (28) it is evident that the hydrodynamic force is composed of two terms, one proportional to the square of the velocity normal to keel and the other proportional to the acceleration normal to the keel. For impacts involving beam-loading coefficients greater than 1 and appreciable chine immersion, the ratio of the acceleration term to the velocity-squared term is usually small. This acceleration term is therefore omitted from the equation of motion, with the result that equation (37), which relates the velocity and draft, is reduced to

$$Q=-\frac{1}{C_\Delta}\int_0^{\zeta'_s/b}\frac{\varphi(\lambda')}{\tan\tau}\frac{m_{w_s}}{\rho b^2}\frac{d\zeta_s}{d\zeta'_s}d\frac{\zeta'_s}{b}$$

which may be written

$$Q=-\frac{k}{C_\Delta} \tag{42}$$

where

$$k=\int_0^{\zeta'_s/b}\frac{\varphi(\lambda')}{\tan\tau}\frac{m_{w_s}}{\rho b^2}\frac{d\zeta_s}{d\zeta'_s}d\frac{\zeta'_s}{b}$$

Omission of the acceleration term from equation (38), which relates the acceleration, velocity, and draft, reduces it to

$$\frac{\ddot{z}b}{\dot{z}_0^2}=-\left(\frac{\dot{z}}{\dot{z}_0}+\kappa\right)^2\frac{\varphi(\lambda')}{C_\Delta\sin\tau}\frac{m_{w_s}}{\rho b^2} \tag{43}$$

Thus, a simplification of the numerical calculation is made possible through the introduction of additional computational charts. One such chart (fig. 7) shows the variation of k with ζ'_s/b for various trims and angles of dead rise. For the flat plate (0° dead rise), k was evaluated by graphical integration after substitution into equation (42) of equations (4), (5), and (23), where $l=\frac{\zeta'_s}{\tan\tau}$, and of the ratio $d\zeta_s/d\zeta'_s$ from figure 6 (b). For the case of finite dead rise, k was similarly evaluated after substitution into equation (42) of equations (4), (6) to (8), (15), and (22) for finite dead rise, where $d\zeta_s/d\zeta'_s$ was taken equal to unity. A second chart was constructed from the variation of the part of equation (43) designated as J, where

$$J=\frac{\varphi(\lambda')}{\sin\tau}\frac{m_{w_s}}{\rho b^2} \tag{44}$$

and is plotted against ζ'_s/b for various trims and angles of dead rise in figure 8.

In order to obtain specific solutions of equations (42) and (43), a computational procedure has been set forth in appendix B. This procedure is somewhat like that outlined for treating equations (37) and (38) and the labor for each solution has been considerably reduced.

EXPERIMENTAL VERIFICATION OF THEORY

MODIFICATION OF THEORY TO PERMIT COMPARISON WITH EXPERIMENT

The theory developed in this report covers free-body landings in which the velocity parallel to the keel is assumed to be constant during impact. The only available experimental data that were usable for verification of this theory however, were obtained during an investigation of constrained models at the Langley impact basin. In these tests the model was mounted on a catapulted carriage in such a way that the model was free to move vertically but was constrained to move with the carriage in a horizontal direction. Since the carriage was several times as heavy as the model, the forward velocity of the carriage-model combination remained approximately constant. In order to compare the theory of this report with the available data, it was necessary to modify the equations so that the velocity component in the horizontal direction, instead of the component in the direction parallel to the keel, was considered constant during impact. The equation of motion was then solved by a procedure similar to that used in deriving the proposed free-body theory with the following results.

The equation relating the velocity of the body to its draft, which is comparable to equation (37), is

$$Q_L=-\cos^3\tau\int_0^{\zeta'_s/b}\frac{\frac{m_{w_s}}{\rho b^2}\frac{d\zeta_s}{d\zeta'_s}d\frac{\zeta'_s}{b}}{\frac{C_\Delta\tan\tau}{\varphi(\lambda')\cos^2\tau}+\int_0^{\zeta'_s/b}\frac{m_{w_s}}{\rho b^2}d\frac{\zeta'_s}{b}} \tag{45}$$

where

$$Q_L\equiv\log_e\frac{\frac{\dot{z}}{\dot{z}_0}+\kappa_L}{1+\kappa_L}+\frac{\kappa_L}{\frac{\dot{z}}{\dot{z}_0}+\kappa_L}-\frac{\kappa_L}{1+\kappa_L}$$

and

$$\kappa_L=\frac{\tan\tau}{\tan\gamma_0}$$

The equation relating the acceleration of the body to its velocity and draft, which is comparable to equation (38), is

$$\frac{\ddot{z}b}{\dot{z}_0^2}=-\frac{\left(\frac{\dot{z}}{\dot{z}_0}+\kappa_L\right)^2\cos\tau\frac{m_{w_s}}{\rho b^2}}{\frac{C_\Delta\tan\tau}{\varphi(\lambda')\cos^2\tau}+\int_0^{\zeta'_s/b}\frac{m_{w_s}}{\rho b^2}d\frac{\zeta'_s}{b}} \tag{46}$$

Specific solutions for impacts may be obtained with these equations as was done with equations (37) and (38). The value of Q_L can be obtained from figure 5 in place of Q when κ_L is substituted for κ.

The omission of the force term arising from acceleration of the deflected mass is handled as in the derivation of the free-body theory and leads to the following equations which are similar to equations (42) and (43): Equation (45), which relates velocity and draft, is reduced to

$$Q_L=-\frac{\cos^4\tau}{C_\Delta}\int_0^{\zeta'_s/b}\frac{\varphi(\lambda')}{\tan\tau}\frac{m_{w_s}}{\rho b^2}\frac{d\zeta_s}{d\zeta'_s}d\frac{\zeta'_s}{b} \tag{47}$$

and equation (46), which relates the acceleration, velocity, and draft, is reduced to

$$\frac{\ddot{z}b}{\dot{z}_0^2}=-\left(\frac{\dot{z}}{\dot{z}_0}+\kappa_L\right)^2\frac{\varphi(\lambda')}{C_\Delta}\frac{\cos^4\tau}{\sin\tau}\frac{m_{w_s}}{\rho b^2} \tag{48}$$

Specific impact solutions of these equations may be obtained as was done in appendix B with equations (42) and (43) for the free-body case.

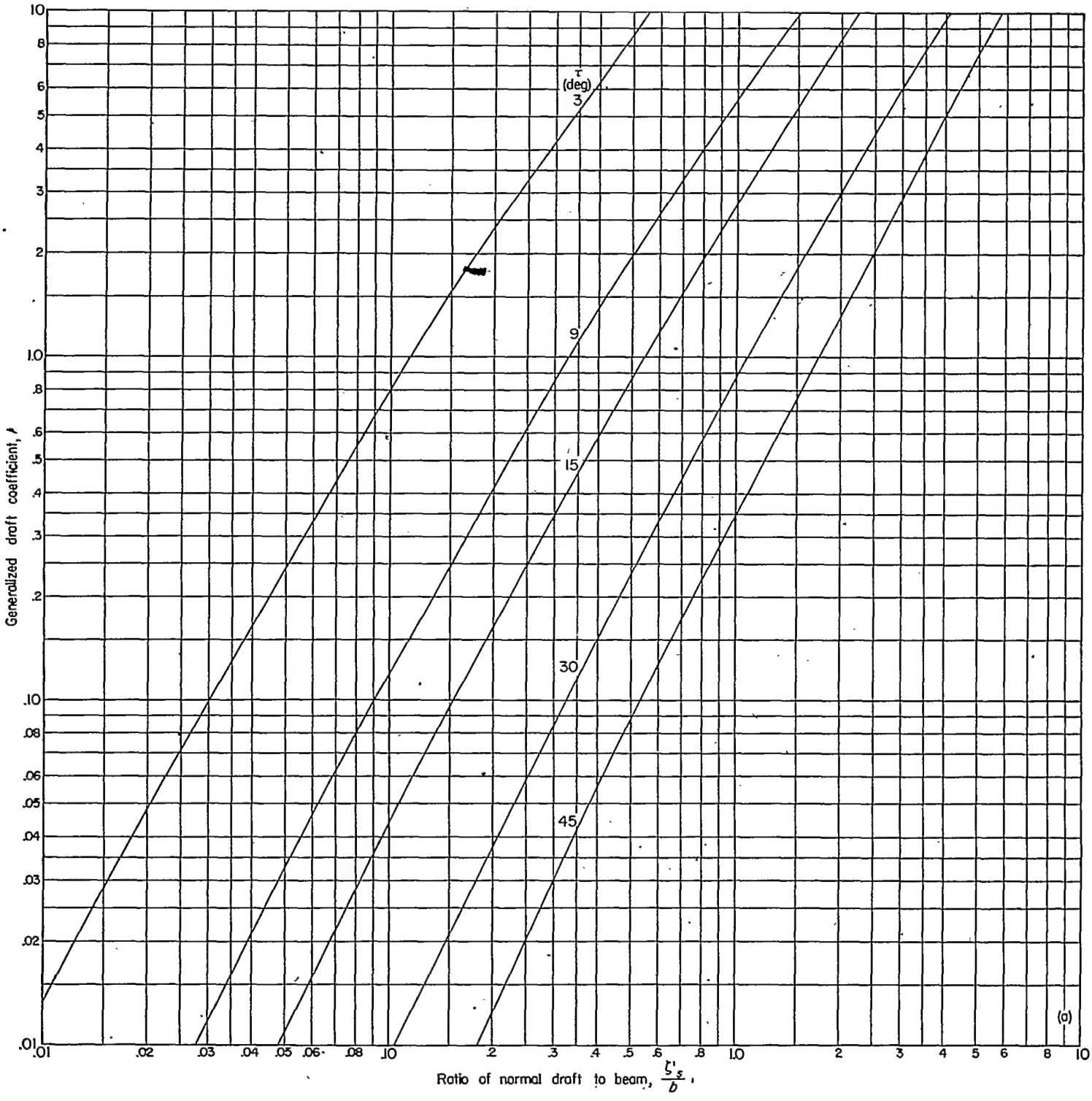

(a) $\beta=0°$.

FIGURE 7.—Variation of generalized draft coefficients for various angles of dead rise.

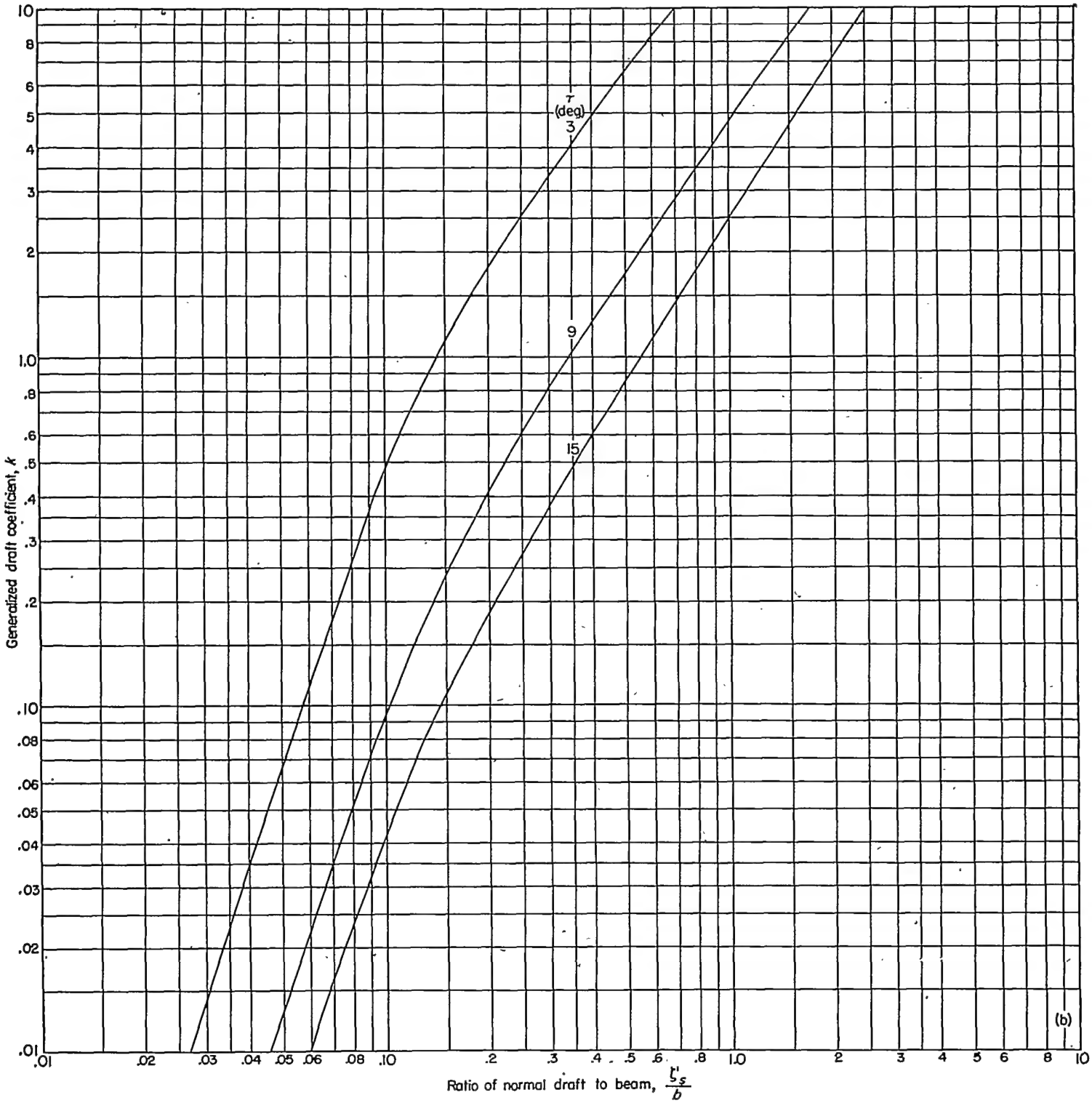

(b) $\beta=10°$.

FIGURE 7.—Continued.

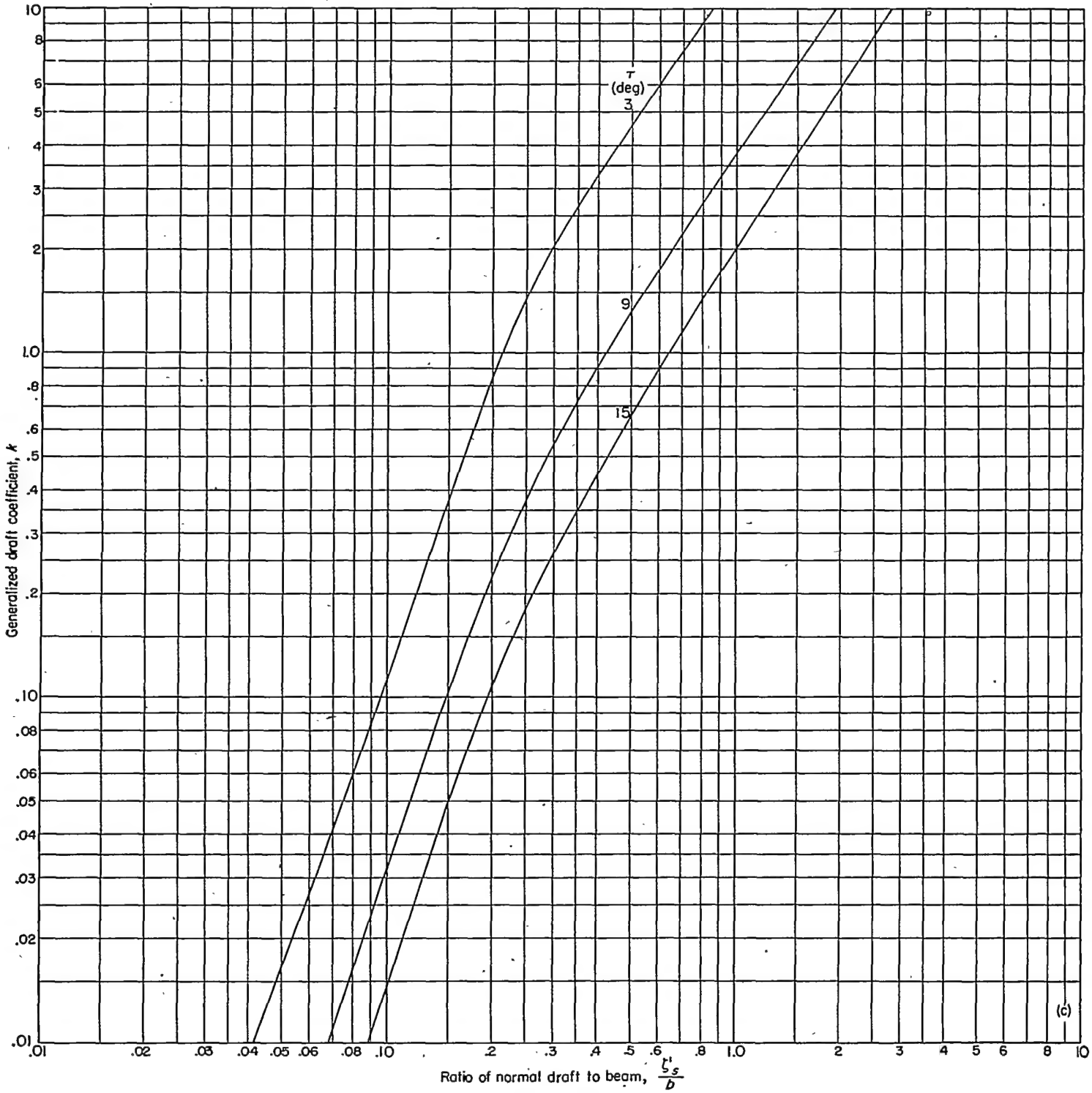

(c) $\beta=20°$.

FIGURE 7.—Continued.

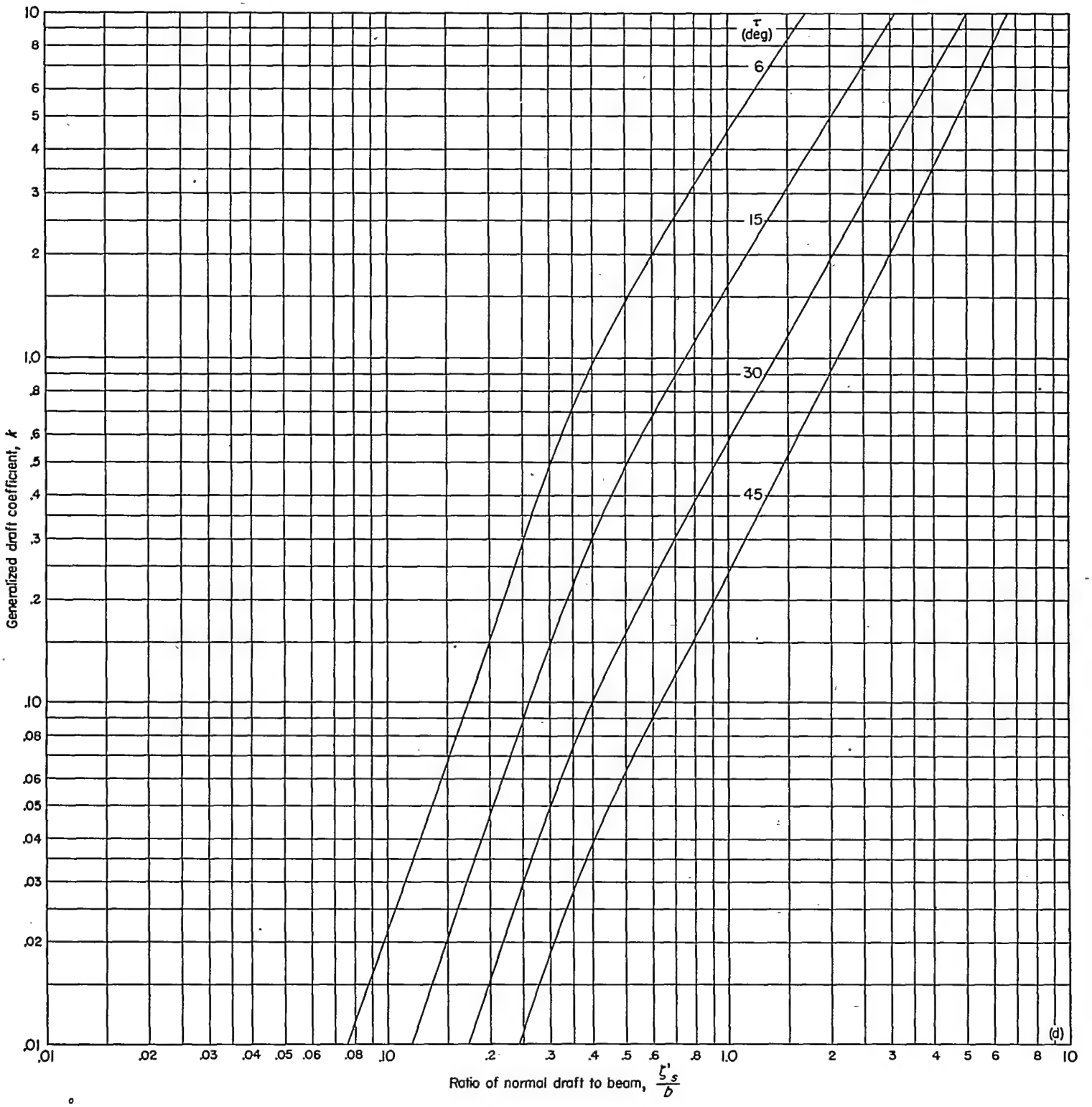

(d) $\beta=30°$.

FIGURE 7.—Concluded.

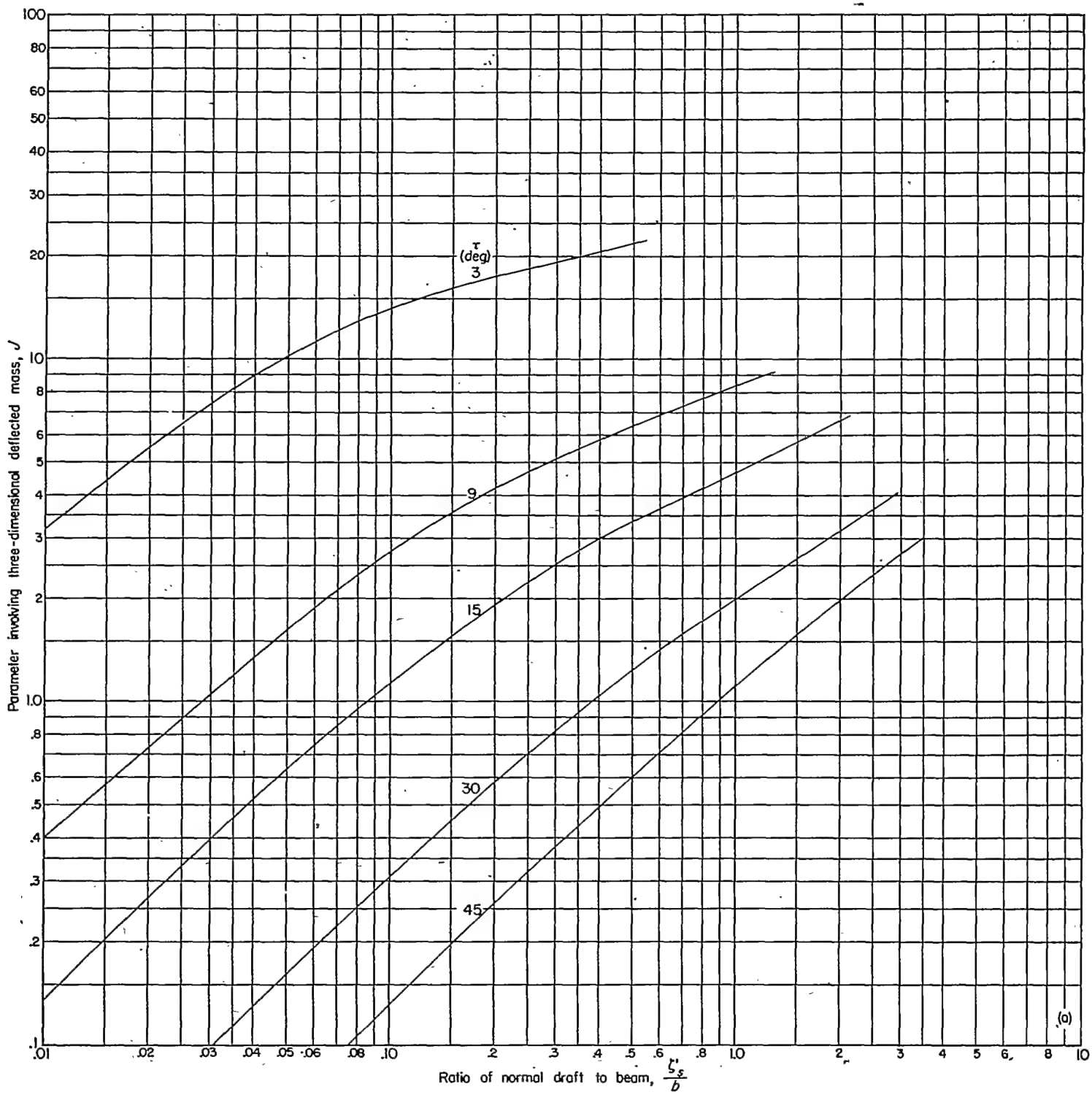

(a) $\beta=0°$.

FIGURE 8.—Variation of parameter involving three-dimensional deflected mass for various angles of dead rise.

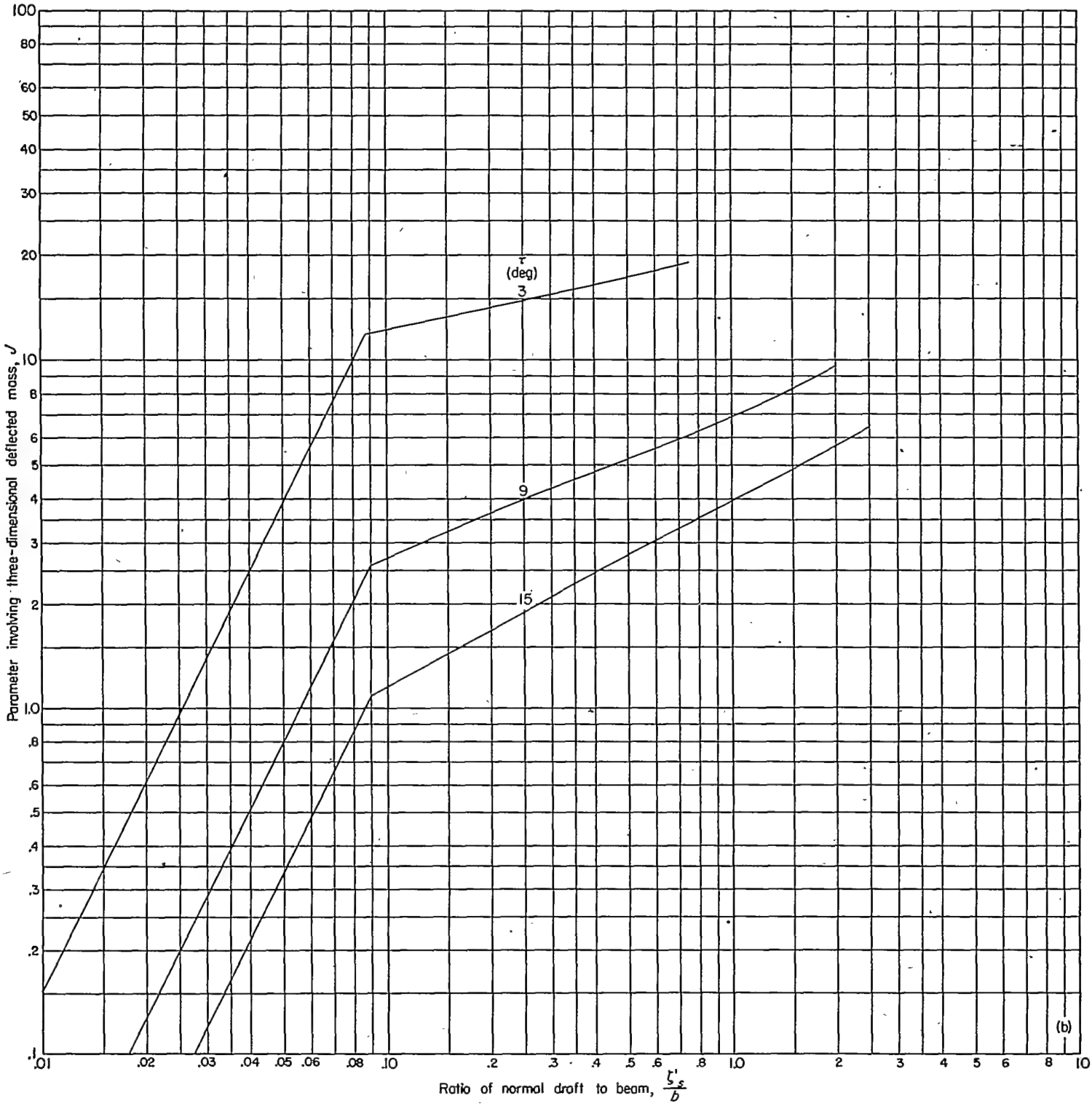

(b) $\beta=10°$.

FIGURE 8.—Continued.

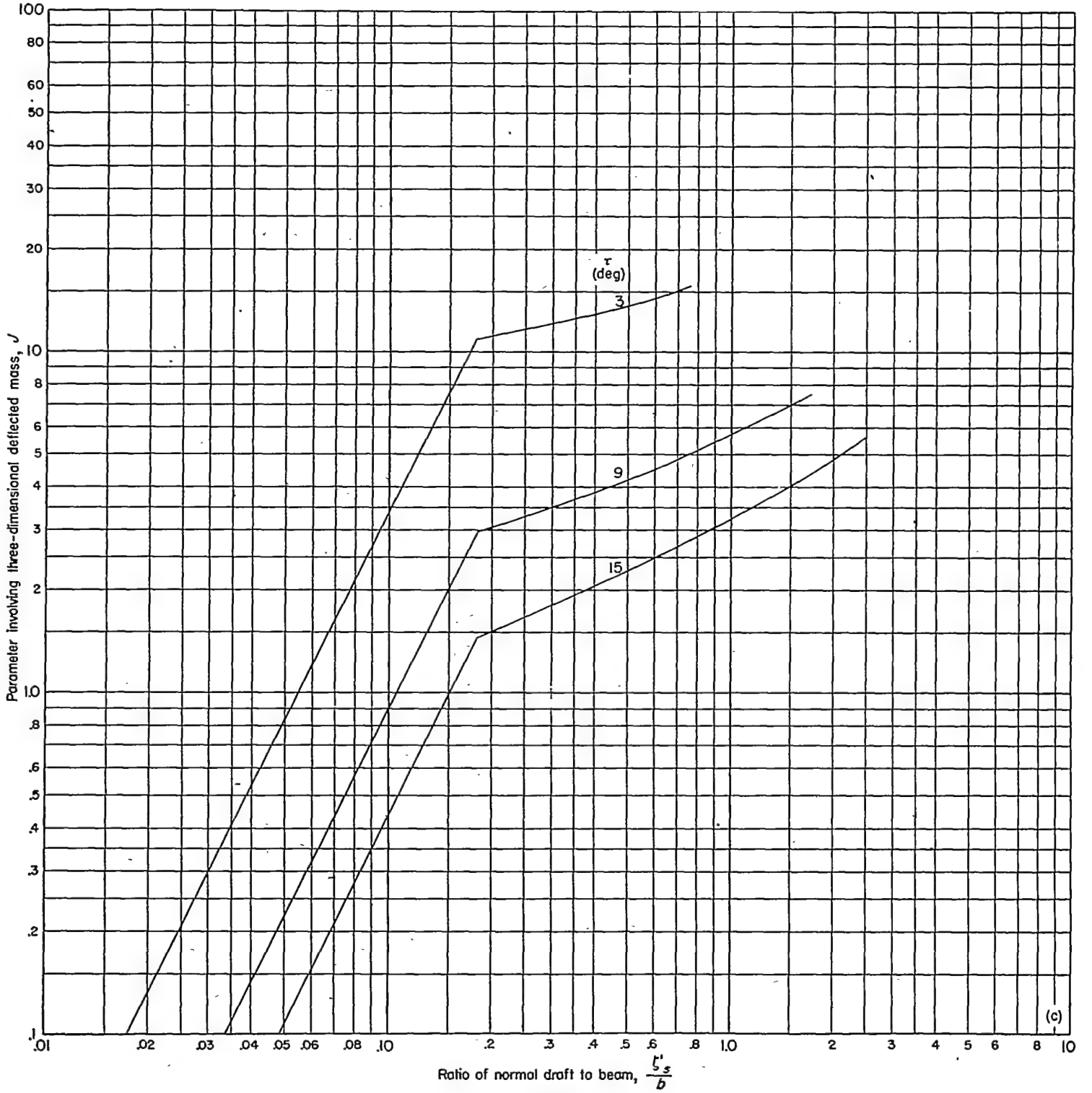

(c) $\beta=20°$.

FIGURE 8.—Continued.

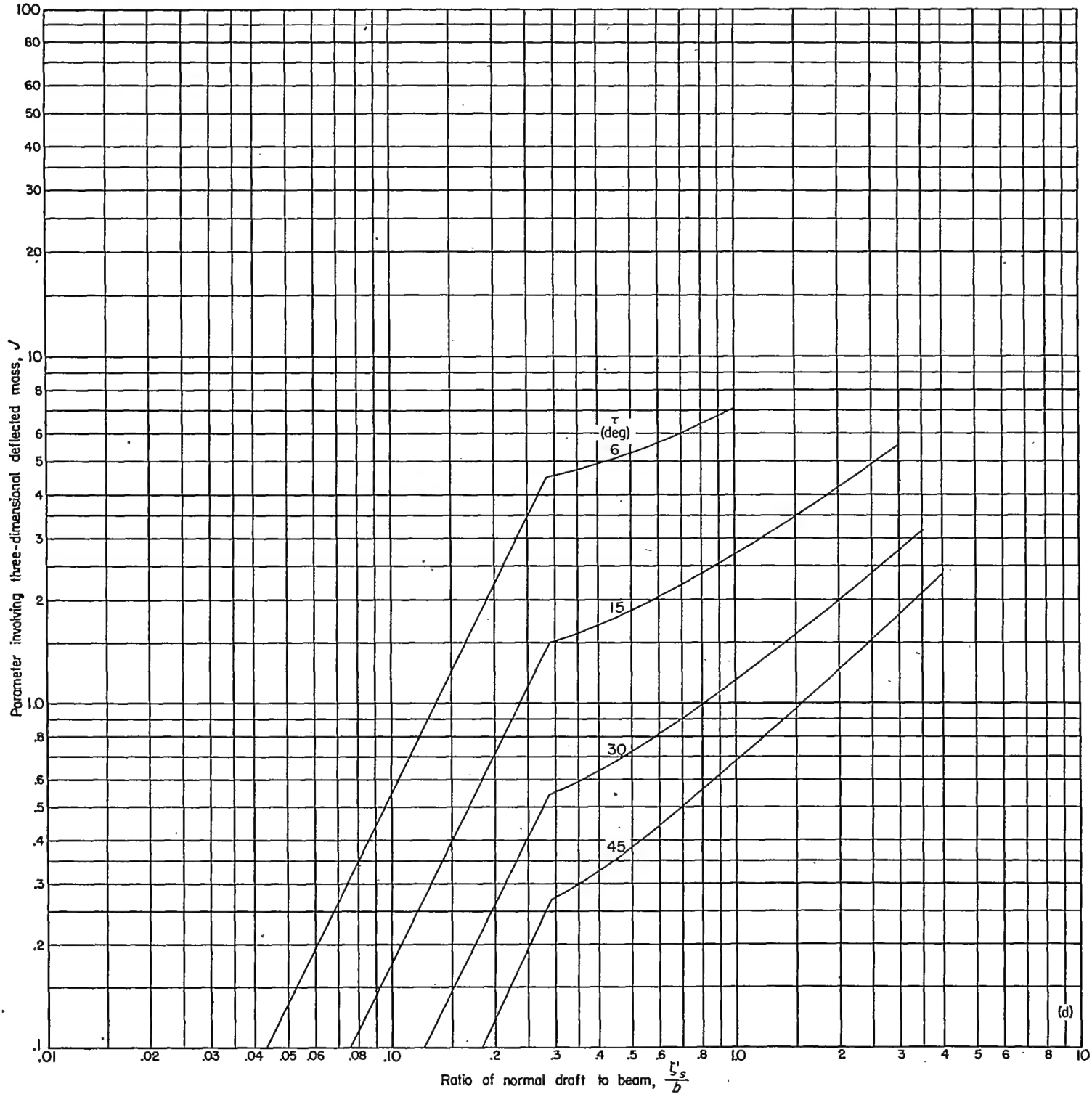

(d) $\beta=30°$.

FIGURE 8.—Concluded.

COMPARISON WITH TEST DATA

Theoretical curves, usable for actual landing-impact calculations, are presented in figures 2 to 8 and were discussed in detail in the previous sections. The succeeding figures present comparisons of experimental data, obtained at the Langley impact basin, with the proposed theory modified for constant forward velocity.

Several theoretical variations of impact load factor, vertical velocity, and vertical displacement with time are compared with experiment in figures 9 and 10. The experimental data in these plots were obtained at the Langley impact basin, and, although a portion of these data is unpublished, the rest may be found in references 13 and 14. In figures 9 (a) and 9 (b) are presented theoretical and experimental load-factor time histories of landings of a flat plate for a wide difference of trim and flight-path angle and for a beam-loading coefficient of 18.8. Fair agreement exists in each case.

An indication of the agreement between theory and experiment at the upper limit of the flight-path angle is given in figures 9 (c) and 9 (d). These figures present theoretical and experimental load-factor time histories for water landings of a flat plate having a beam-loading coefficient of 18.8 at trims of 6° and 15° for the end-point case of a vertical drop (flight-path angle of 90°). Fair agreement is also obtained in these figures.

In order to demonstrate the effect of neglecting the force term arising from the acceleration of the deflected mass, figure 9 (e) is presented for the landing of a flat plate with a medium beam-loading coefficient of 4.36, at the lowest trim for which data were available. The difference between the two theoretical lines plotted illustrates the effect of neglecting this acceleration term. The higher line represents the solution with the deflected-mass acceleration neglected, and at maximum acceleration the difference between the two theoretical curves is seen to be about 10 percent. The deflected mass used in the acceleration term may possibly be overestimated here. If the cylindrical virtual water mass based on the beam as a diameter (ref. 2) were used instead, this difference of 10 percent would be somewhat reduced. The experimental data fall somewhere between the two curves, but no conclusion is drawn from this fact since the possible errors in the experimental data are estimated to be of the order of magnitude of $\pm 0.2g$.

The effect of water rise at the keel is demonstrated in figure 9 (f). This effect is greatest for small immersions and is therefore important for lightly loaded plates for which maximum drafts in impact are small. The upper curve includes the effect of water rise at the keel and the lower one does not. For plates with medium loading, consideration of this water rise increases the theoretical maximum load by about 9 percent and increases the initial rate of load application, so that the time to maximum load is reduced. As in figure 9 (e), the experimental data fall between the two theoretical curves up to maximum acceleration and the same reservation concerning accuracy holds. It might be mentioned that the acceleration data presented in this report have a time lag which is estimated to be approximately 0.005 second. If this also is taken into account, the theory including water rise in figure 9 (f) would give better agreement with the experimental data up to maximum load than the theory omitting water rise.

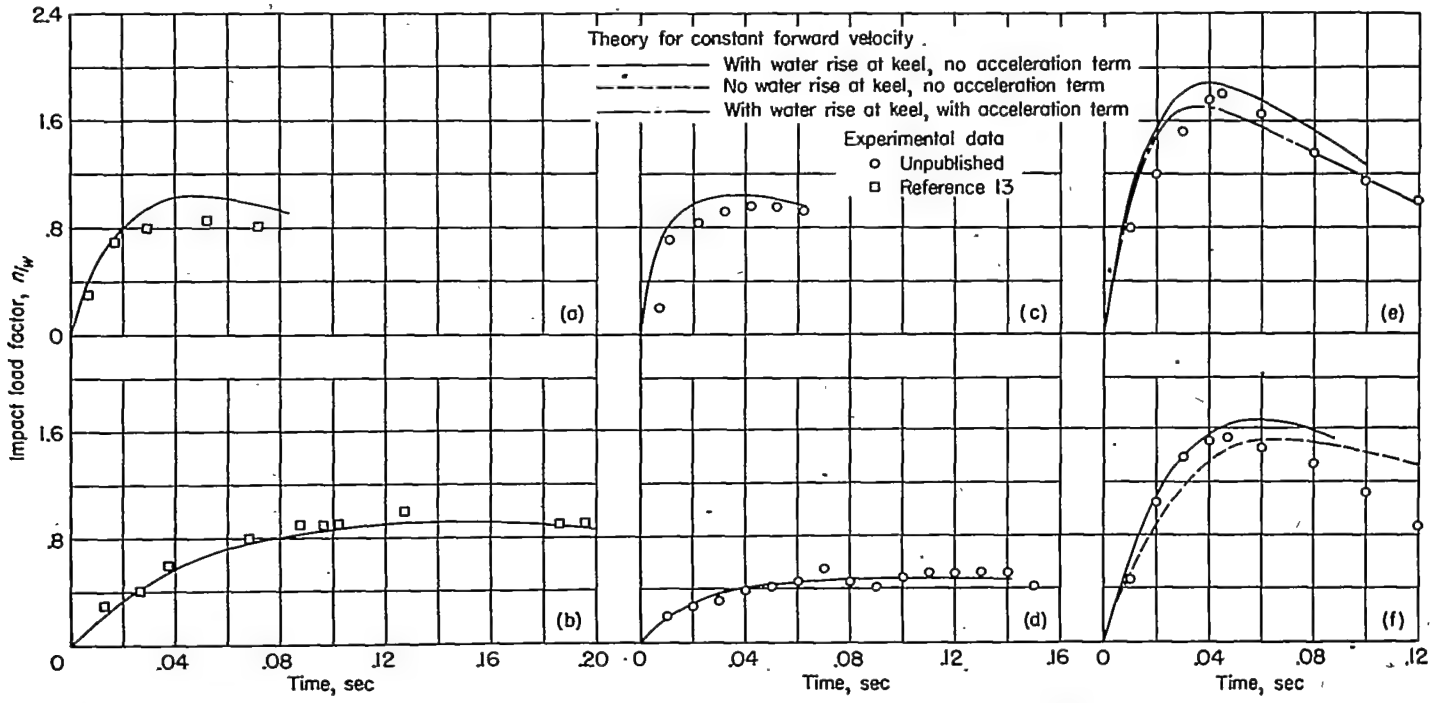

(a) Sample time history. $\tau=6°$; $\gamma_0=2.1°$; $\dot{z}_0=2.9$ feet per second; $C_\Delta=18.8$.

(b) Sample time history. $\tau=30°$; $\gamma_0=21.2°$; $\dot{z}_0=9.1$ feet per second; $C_\Delta=18.8$.

(c) Sample time history. $\tau=6°$; $\gamma_0=90°$; $\dot{z}_0=9.4$ feet per second; $C_\Delta=18.8$.

(d) Sample time history. $\tau=15°$; $\gamma_0=90°$; $\dot{z}_0=9.56$ feet per second; $C_\Delta=18.8$.

(e) Effect of acceleration. $\tau=9°$; $\gamma_0=8.12°$; $\dot{z}_0=6.06$ feet per second; $C_\Delta=4.36$.

(f) Effect of water rise. $\tau=15°$; $\gamma_0=5.55°$; $\dot{z}_0=4.86$ feet per second; $C_\Delta=4.36$.

FIGURE 9.—Comparisons of theoretical and experimental impact-load time histories for flat plate.

Figure 10 (a) presents time histories of impact load factor, vertical velocity, and draft for an impacting flat plate having a beam-loading coefficient of 18.8. The effects of neglecting the acceleration of the deflected mass and water rise at the keel are again shown here, in addition to the effect of a large carriage mass. Comparison of the theoretical curves for free motion and constant forward velocity indicates that the large test-carriage mass, which causes the horizontal velocity to approach a constant value, increases the maximum load factor for this case by about 3 percent. The increase becomes considerably larger for the higher trims. The effects of carriage mass, acceleration of the deflected mass, and water rise at the keel on vertical velocity and draft are seen to be small.

In figure 10 (b), time histories of impact load factor, vertical velocity, and draft are presented for an impact of a hull with an angle of dead rise of 30° and a beam-loading coefficient of 18.8. The small effect of acceleration of the deflected mass may be noted by comparing the two curves and the experimental data on each plot of this figure. The agreement between the theoretical and experimental hull load factors would be improved if the aforementioned 0.005-second time lag were taken into account. A similar time lag exists in the vertical-velocity data and, although the exact value of this lag is unknown, it has been roughly estimated at 0.005 to 0.01 second. If this lag were taken into account, the agreement between the theoretical and the experimental velocity would be considerably improved. If more were known about the water rise at the keel for the float with dead rise and if a better variation of two-dimensional deflected mass were available, the agreement would probably be further improved. Thus, from figures 9 and 10 the agreement between theoretical and experimental time histories is seen to be fair.

The variation of impact lift coefficient with flight-path angle for wide ranges of trim and beam-loading coefficient is shown in figure 11 for 0° dead-rise angle and for flight-path angles up to 21.5°. The experimental data in this figure

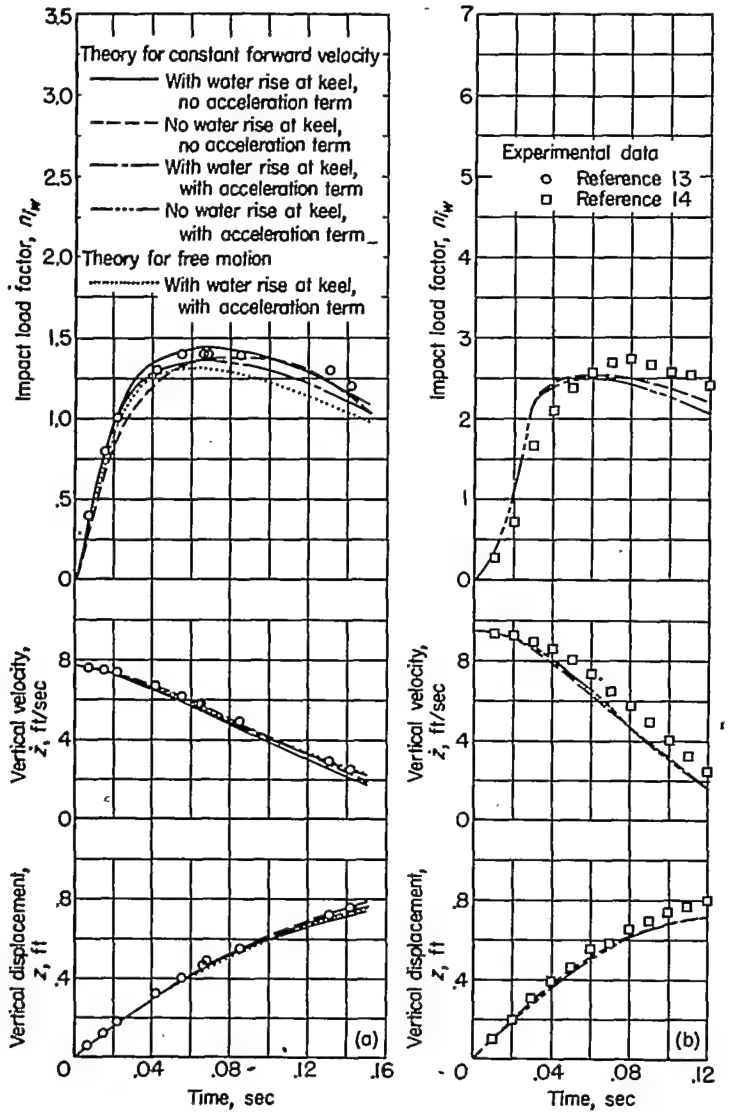

(a) $\beta=0°$; $\tau=15°$; $\gamma_0=10.1°$; $\dot{z}_0=7.7$ feet per second; $C_\Delta=18.8$.

(b) $\beta=30°$; $\tau=15°$; $\gamma_0=5.92°$; $\dot{z}_0=9.4$ feet per second; $C_\Delta=18.8$.

FIGURE 10.—Comparisons of theoretical and experimental impact time histories for 0° and 30° angles of dead rise.

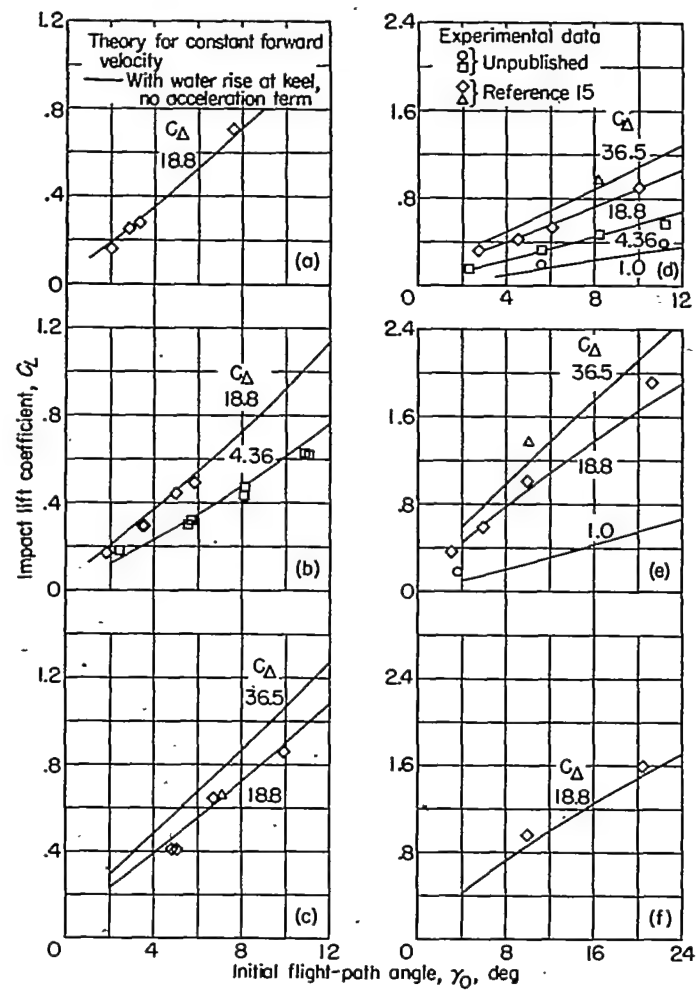

(a) $\tau=6°$.
(b) $\tau=9°$.
(c) $\tau=12°$.
(d) $\tau=15°$.
(e) $\tau=30°$.
(f) $\tau=45°$.

FIGURE 11.—Comparisons of theoretical and experimental impact lift coefficients C_L for a flat plate at various beam loadings.

$$C_L=\frac{(n_{t_w})_{max}W}{\frac{\rho}{2}b^2V_0^2}$$

were obtained at the Langley impact basin and the published portion may be found in reference 15. Fair agreement is seen to exist between experiment and the theory that incorporates water rise at the keel, omits the acceleration term, and assumes constant horizontal velocity, at least for beam-loading coefficients greater than 1. For beam-loading coefficients less than 1, the effects of acceleration and of flight-path angle on the deflected mass might introduce noticeable errors.

Since fair agreement was demonstrated between theoretical and experimental flat-plate landing accelerations for flight-path angles up to 21.5° in figure 11 and for the end point of 90° flight-path angle in figures 9 (c) and 9 (d), the proposed theory is believed to be applicable for all flight-path angles.

The variation of impact lift coefficient with flight-path angle for an angle of dead rise of 30°, a beam-loading coefficient of 18.8, and a wide range of trim is presented in figure 12. The solid curves represent the suggested theory for constant forward velocity including water rise at the keel and neglecting the acceleration term, with $d\zeta_s/d\zeta'_s$ taken as 1 for the body with dead rise. The dashed lines are calculated from the theory of reference 2, which predicts the occurrence of maximum load at the instant of chine immersion for impacts involving deep immersion of the chines. Each of these curves experiences a radical change of slope and shape at a certain critical flight-path angle for each trim and beam loading. For flight-path angles below this critical value, maximum load occurs prior to chine immersion. For a short range of flight-path angles immediately above this critical value, maximum load is believed to occur at or near chine immersion, and for high flight-path angles, maximum load occurs subsequent to chine immersion. Since the variation of deflected mass with draft is different before and after chine immersion, a break in the curve is expected to occur at the point of chine immersion. In figure 12 a comparison of the two theories with experimental data from reference 14 shows that for impacts involving a small degree of chine immersion the theory of reference 2 gives better results, at least for low trims, whereas for impacts involving deeply immersed chines the agreement with the theory suggested in this report is better. This disagreement of the suggested theory with experiment for small degrees of chine immersion when dead rise is present could be improved through use of a more accurate deflected-mass variation in the region of chine immersion. The general agreement between the experimental data for bodies with dead rise and the proposed theory, however, is seen to be fair, even for small amounts of chine immersion where the theory is conservative.

The variation of maximum draft with flight-path angle is presented in figure 13 for angles of dead rise of 0° and 30° and for several trims and beam loadings. The general agreement with data from the Langley impact basin, the published portion of which may be found in references 14 and 15, is seen to be fair. This agreement indicates that the theory of the present report could be used in conjunction with the method of reference 16 to compute pitching-moment time histories during landing impacts.

CONCLUSIONS

A method has been derived for the analytical determination of the motions and hydrodynamic loads in chine-immersed water landings of prismatic bodies. Comparison of this theoretical work with other available theory and with experimental data obtained at the Langley impact basin has led to the following conclusions:

1. In general, the concept of a two-dimensional deflected mass with a correction for three-dimensional flow can be

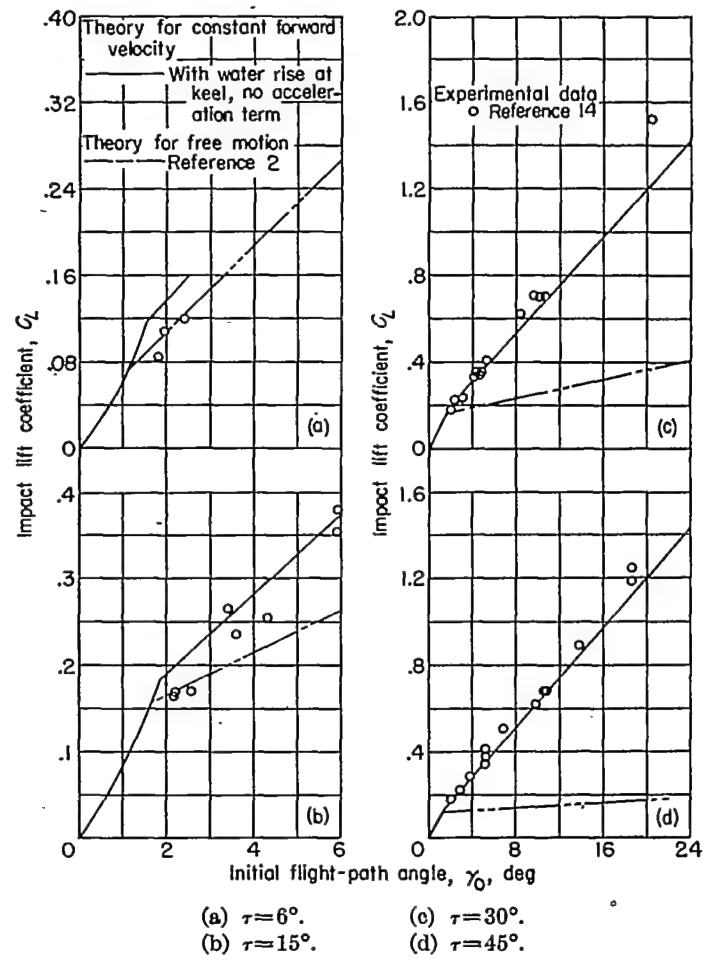

(a) $\tau=6°$. (c) $\tau=30°$.
(b) $\tau=15°$. (d) $\tau=45°$.

FIGURE 12.—Comparisons of theoretical and experimental impact lift coefficients for a hull with an angle of dead rise of 30° and a beam-loading coefficient of 18.8. $C_L=\dfrac{(n_{i_w})_{max}W}{\frac{\rho}{2}b^2V_0^2}$.

used to predict with reasonable accuracy the loads and motions during landings of prismatic bodies involving immersion of the chines.

2. Use of Wagner's virtual-mass variation for non-chine-immersed sections combined with a deflected-mass variation obtained from Bobyleff's solution after chine immersion of these sections, with level water as a boundary, gives fair agreement with experiment for deep impacts.

3. For shallow impacts at the lower trims, involving slight chine immersion of bodies with dead rise, the virtual-mass variation suggested in NACA TN 1516 gives better agreement with experiment than the proposed variation.

4. The effects of water rise at the keel in the case of a flat plate and the effects of the ratio of test-carriage mass to model mass in the general case are significant enough to be included in the proposed equations of motion.

5. Omission of the force arising from acceleration of the deflected mass is not serious for beam-loading coefficients larger than unity and results in a large reduction in the work required for each solution.

LANGLEY AERONAUTICAL LABORATORY,
NATIONAL ADVISORY COMMITTEE FOR AERONAUTICS,
LANGLEY FIELD, VA., *June 25, 1952.*

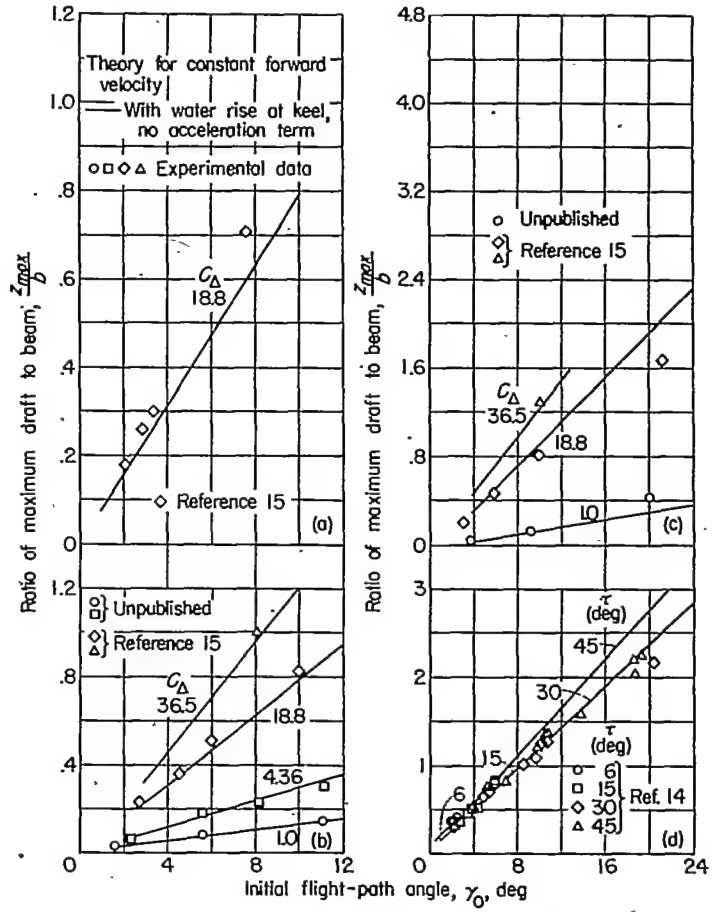

(a) $\beta=0°$; $\tau=6°$.
(b) $\beta=0°$; $\tau=15°$.
(c) $\beta=0°$; $\tau=30°$.
(d) $\beta=30°$; $C_\Delta=18.8$.

FIGURE 13.—Comparisons of theoretical and experimental maximum drafts for 0° and 30° angles of dead rise.

APPENDIX A

WATER RISE ON A RECTANGULAR FLAT PLATE

As has been mentioned in this report, reference 13 shows the water rise at the keel of an impacting body to be relatively insensitive to flight-path angle and thus capable of being evaluated from planing data. Since such data are most conveniently analyzed in terms of the wetted length of the body (l in fig. 1) and since this analysis is based on the draft z with respect to the undisturbed water surface, the relation between these two quantities must be obtained. This relation is expressed by the equation (see fig. 1)

$$z=l \sin \tau - r \tag{A1}$$

where r is the water rise at the keel.

Several papers about planing discuss this phenomenon of water rise at the keel in connection with steady motion and reference 13 discusses it in connection with motion of the peak-pressure line during impact. A theoretical solution by Wagner (ref. 10) for the two-dimensional planing flat plate predicts infinite water rise for the ideal case, in which gravity and viscosity are neglected. Planing data from references 17 to 19 show the increase in wetted length due to water rise $\lambda'-\lambda$ to be a more or less constant fraction of the hull beam, with only a small variation due to changes in trim. At low length-beam ratios this result is more or less in agreement with Wagner's theory for planing, but it would not be in agreement for impact, as indicated in reference 13. This reference shows an expected gradual transition from no water rise at the instant of water contact to some constant value for the hull tested at ratios of wetted length to beam greater than 1.5. The rise variation of reference 13 is not used in this report, however, since it is based on the peak-pressure location and not on the measured wetted length. The following system is therefore used for the flat plate. The case of a hull with dead rise is not covered because of a lack of sufficient information on water rise at the keel in planing.

The assumption is made, as in reference 13, that the water rise at the keel for a two-dimensional flow about an impacting plate of infinite width is independent of the flight-path angle and is proportional to the draft; thus

$$r=Cz \tag{A2}$$

where r is the rise and C is the constant of proportionality. In nondimensional form this becomes

$$\frac{r}{b}=C\lambda \sin \tau \tag{A3}$$

where $\lambda=\frac{z}{b \sin \tau}$ is the length-beam ratio below the undisturbed water surface for a flat plate. For three-dimensional flow about plates with a very small ratio of wetted length to beam, equation (A3) would also be applicable. However, as the length-beam ratio increases, this piled-up water should be relieved through flow around the sides of the model. Thus, some form of correction for three-dimensional flow $f(\lambda)$ is required to reduce the rise for high length-beam ratios, as follows:

$$\frac{r}{b}=C\lambda f(\lambda) \sin \tau \tag{A4}$$

A correction for three-dimensional flow which fits the end points, reducing equation (A4) to equation (A3) at small length-beam ratios and to a constant value at large length-beam ratios, is Pabst's correction (eq. (4) in the body of the report) applied to the inverse hydrodynamic aspect ratio. Substituting this correction into equation (A4) gives

$$\frac{r}{b}=C\lambda\varphi\left(\frac{1}{\lambda}\right) \sin \tau \tag{A5}$$

The effective ratio of wetted draft to beam (see fig. 1) is therefore

$$\frac{z+r}{b}=\frac{z}{b}+C\lambda\varphi\left(\frac{1}{\lambda}\right) \sin \tau \tag{A6}$$

Since $\lambda=\frac{z}{b \sin \tau}$ and $\lambda'=\frac{z+r}{b \sin \tau}$, the effective ratio of wetted length to beam is

$$\lambda'=\lambda\left[1+C\varphi\left(\frac{1}{\lambda}\right)\right] \tag{A7}$$

An average value of 0.4 for C was obtained from the experimental planing data in references 17 to 19. Figure 6(a) is a plot of equation (A7) based on this value of C, and figure 6(b) is a plot of the slope of this curve, or $\frac{d\lambda}{d\lambda'}=\frac{d\zeta_s}{d\zeta'_s}$ against λ'.

APPENDIX B

SUGGESTED COMPUTATIONAL PROCEDURE

This section gives suggested computational methods to facilitate calculation of loads and motions during free-body impacts of a prismatic form experiencing appreciable chine immersion. These methods are based on a solution of the equation of motion which takes into account water rise at the keel, neglects the acceleration of the virtual mass, and neglects the effects of flight-path angle on water rise at the keel and on the normal-force coefficient. As a result of these omissions, the effects of which are small at the higher beam loadings, this solution is considered applicable only to those cases for which the beam-loading coefficient exceeds unity. This applicability is also restricted to drafts for which the leading edge of the prismatic surface has not penetrated beneath the water surface.

The overall computational procedure is subdivided into four less-general procedures to increase the utility of the solution. The first of these treats smooth-water landings of prismatic bodies approximating V-sections and makes use of computational charts covering specific angles of dead rise of 0°, 10°, 20°, and 30° and certain fixed trims. The second procedure applies to the same bodies for all practical angles of dead rise and fixed trims but requires more work for each solution. The third procedure covers prismatic bodies of arbitrary shape but requires experimental data from planing or drop tests. The fourth procedure accomplishes a conversion from smooth-water to rough-water landings. Explanation of symbols is given in the list of symbols following the introduction and in figure 1.

PROCEDURE 1—SMOOTH-WATER LANDINGS OF A PRISMATIC BODY HAVING A CROSS SECTION APPROXIMATING A V-SHAPE WITH A DEAD-RISE ANGLE OF 0°, 10°, 20°, OR 30° AT ONE OF SEVERAL FIXED TRIMS

1. Obtain a value of κ from figure 4 through use of appropriate values of initial flight-path angle γ_0 and trim τ.

2. Select several values of the vertical-velocity ratio $\dot{z}/\dot{z}_0$ between 1 and -1 and, with the value of κ, obtain a value of Q from figure 5 for each value of $\dot{z}/\dot{z}_0$.

3. Compute a value of k for each value of Q from the equation $k=-C_\Delta Q$, where $C_\Delta=\dfrac{W}{\rho g b^3}$ and is defined as the beam-loading coefficient.

4. Obtain values of the ratio of normal draft to beam ζ'_s/b for each value of k from the curve for the appropriate values of τ and average angle of dead rise β in figure 7.

5. Obtain a value of J for each value of ζ'_s/b for the appropriate values of τ and β in figure 8.

6. Calculate a value of the nondimensional acceleration $\ddot{z}b/z_0^2$ for each combination of $\dot{z}/\dot{z}_0$ and ζ'_s/b through substitution of the appropriate quantities into the equation

$$\frac{\ddot{z}b}{\dot{z}_0^2}=-\left(\frac{\dot{z}}{\dot{z}_0}+\kappa\right)^2\frac{J}{C_\Delta} \tag{B1}$$

7. Plot the load factor $n_{i_w}=-\dfrac{\ddot{z}}{g}$ and the vertical velocity $\dot{z}$ against the ratio of normal draft to beam ζ'_s/b.

8. Repeat steps 1 to 7 for several other values of γ_0 and τ, covering the range of interest.

9. Compute values of $C_L=\dfrac{(n_{i_w})_{max}\ W}{\frac{\rho}{2}\dot{b}^2 V_0^2}$ from the maximum values of n_{i_w} obtained from the curves obtained in step 8 and plot C_L against γ_0 for various values of τ. The resulting curves may be used as design curves.

10. Compute values of draft-beam ratio z/b from the equation

$$\frac{z}{b}=\frac{\zeta'_s}{b}\frac{\lambda}{\lambda'}\cos\tau \tag{B2}$$

where λ/λ' is obtained from figure 6(a) for $\beta=0°$ and is taken as unity for $\beta\geqq 10°$. For the case where $\beta=0°$, $\lambda'=\dfrac{\zeta'_s}{b\tan\tau}$.

11. For calculation of structural response, the time variation from water contact through exit may be found by incremental graphical integration of the equation

$$\frac{tV_0}{b}=\frac{1.}{\sin\gamma_0}\left(\int_0^{z_1/b}\frac{d\frac{z}{b}}{\frac{\dot{z}}{\dot{z}_0}}+\int_{\dot{z}_1/\dot{z}_0}^{\dot{z}_2/\dot{z}_0}\frac{d\frac{\dot{z}}{\dot{z}_0}}{\frac{\ddot{z}b}{\dot{z}_0^2}}+\int_{z_2/b}^{z/b}\frac{d\frac{z}{b}}{\frac{\dot{z}}{\dot{z}_0}}\right)$$

where V_0 is the initial resultant velocity at water contact. The first integral gives the time to some point prior to maximum draft, the second includes maximum draft, and the third covers the remaining time to exit. Although the first and third integrals give the time as a function of draft and the second gives it as a function of vertical velocity, the previously derived relationships between draft, vertical velocity, and load factor allow the time histories of all of these quantities to be computed.

PROCEDURE 2—SMOOTH-WATER LANDINGS OF A PRISMATIC BODY HAVING A CROSS SECTION APPROXIMATING A V-SHAPE WITH ANY DEAD-RISE ANGLE, AT ANY TRIM

1. Select a series of several values of the ratio of normal draft to beam ζ'_s/b and compute values of $m_{w_s}/\rho b^2$ from the equations

$$\frac{m_{w_s}}{\rho b^2}=\frac{\pi^3}{32}+0.44\frac{\zeta'_s}{b} \qquad (\beta=0°)$$

$$\frac{m_{w_s}}{\rho b^2}=\frac{\pi}{2}\left[\frac{\zeta'_s}{b}f(\beta)\right]^2 \qquad \left(\beta>0°;\frac{\zeta'_s}{b}\leqq\frac{\tan\beta}{2}\right)$$

$$\frac{m_{w_s}}{\rho b^2}=\frac{\pi}{8}[f(\beta)\tan\beta]^2+\frac{B}{2}\left(\frac{\zeta'_s}{b}-\frac{\tan\beta}{2}\right) \qquad \left(\beta>0°;\frac{\zeta'_s}{b}>\frac{\tan\beta}{2}\right)$$

where

$$f(\beta)=\frac{\pi}{2\beta}-1$$

and a value of B is obtained from figure 3 by means of the average angle of dead rise β.

2. Obtain a value of λ' for each value of ζ'_s/b selected in step 1 by means of the equations

$$\lambda'=\frac{\zeta'_s}{b\tan\tau} \qquad (\beta=0°) \tag{B3}$$

$$\lambda'=\frac{1}{\tan\tau f(\beta)} \qquad \left(\beta>0°;\frac{\zeta'_s}{b}=\frac{\zeta_s}{b}\leqq\frac{\tan\beta}{2}\right) \tag{B4}$$

$$\lambda'=\frac{\left(\frac{\zeta'_s}{b}\right)^2}{\tan\tau\left[\frac{\zeta'_s}{b}-\frac{1}{4f(\beta)}\right]} \qquad \left(\beta>0°;\frac{\zeta'_s}{b}=\frac{\zeta_s}{b}>\frac{\tan\beta}{2}\right) \tag{B5}$$

and substitute these values of λ' into figure 2 to obtain values of $\varphi(\lambda')$.

3. Obtain values of $d\zeta_s/d\zeta'_s$ from figure 6(b) for each value of λ' for cases where $0°\leqq\beta<10°$. For cases where $\beta\geqq10°$, $d\zeta_s/d\zeta'_s$ is taken equal to unity.

4. Combine the results of steps 1 to 3 to obtain values of $\frac{\varphi(\lambda')}{\tan\tau}\frac{m_{w_s}}{\rho b^2}\frac{d\zeta_s}{d\zeta'_s}$, plot these against ζ'_s/b, and graphically evaluate the integral

$$QC_\Delta=-\int_0^{\zeta'_s/b}\frac{\varphi(\lambda')}{\tan\tau}\frac{m_{w_s}}{\rho b^2}\frac{d\zeta_s}{d\zeta'_s}\,d\frac{\zeta'_s}{b} \tag{B6}$$

at each value of ζ'_s/b selected in step 1.

5. Obtain a value of Q from equation (B6) for each value of ζ'_s/b where the beam-loading coefficient $C_\Delta=\frac{W}{\rho g b^3}$. For each value of Q, obtain a value of the vertical-velocity ratio $\dot{z}/\dot{z}_0$ from figure 5, using the value of κ obtained from figure 4 by means of the appropriate initial flight-path angle γ_0 and the value of fixed trim τ.

6. Calculate a value of the nondimensional acceleration $\ddot{z}b/\dot{z}_0^2$ for each combination of $\dot{z}/\dot{z}_0$ and ζ'_s/b through substitution of the appropriate quantities into the equation

$$\frac{\ddot{z}b}{\dot{z}_0^2}=-\left(\frac{\dot{z}}{\dot{z}_0}+\kappa\right)^2\frac{\varphi(\lambda')}{C_\Delta\sin\tau}\frac{m_{w_s}}{\rho b^2}$$

7. 8. 9. 10. 11. Same as in procedure 1.

PROCEDURE 3—SMOOTH-WATER LANDINGS OF A PRISMATIC BODY OF ARBITRARY CROSS SECTION WHERE SECTION CHARACTERISTICS OBTAINED FROM EXPERIMENTAL DATA ARE REQUIRED

This procedure is suggested as a rough approximation only, as it has not been verified by experimental data.

1. Select a series of several values of the ratio of normal draft to beam ζ'_s/b and compute a value of λ' for each value of ζ'_s/b, either from formulas (B3) to (B5) of procedure 2, where β is the average angle of dead rise, or from the equation $\lambda'=\frac{l^2}{S}$ where l is the wetted length and S is the wetted area projected normal to the keel. Obtain a value of $\varphi(\lambda')$ for each value of λ' from figure 2.

2. Substitute data from high-speed planing runs, vertical drops, or oblique impacts of a heavily loaded prismatic body with a cross-sectional shape similar to that of the body of interest into the equation

$$\frac{m_{w_s}}{\rho b^2}=\frac{F_N\tan\tau}{\varphi(\lambda')\dot{\zeta}^2\rho b^2}$$

to obtain a value of $m_{w_s}/\rho b^2$ for each value of ζ'_s/b.

3. 4. 5. 6. Same as in procedure 2.

7. 8. 9. 10. 11. Same as in procedure 1.

PROCEDURE 4—CONVERSION TO ROUGH-WATER STEP LANDINGS

Rough-water landings of prismatic bodies with any angle of dead rise into waves which are long compared with these bodies may be handled as in reference 20 by the following procedure:

1. Determine the wave slope at the point of contact from reference 6, articles 229 and 251, or from reference 20. The most severe landings are believed to occur on the flank of an advancing wave, in the region of the steepest slope.

2. Rotate the space coordinate system so that the z-axis is normal to the wave slope and compute an effective trim with respect to these coordinates.

3. Compute the wave-particle velocity at the point of contact from reference 6, articles 229 and 251, or from reference 20, subtract this velocity vectorially from the hull velocity, and compute an effective flight-path angle from the resultant velocity with respect to the new coordinates.

4. Using these effective values of trim and initial flight-path angle, continue as in smooth-water cases outlined in procedures 1, 2, and 3.

REFERENCES

1. Mayo, Wilbur L.: Analysis and Modification of Theory for Impact of Seaplanes on Water. NACA Rep. 810, 1945. (Supersedes NACA TN 1008.)
2. Milwitzky, Benjamin: A Generalized Theoretical and Experimental Investigation of the Motions and Hydrodynamic Loads Experienced by V-Bottom Seaplanes During Step-Landing Impacts. NACA TN 1516, 1948.
3. Milwitzky, Benjamin: A Theoretical Investigation of Hydrodynamic Impact Loads on Scalloped-Bottom Seaplanes and Comparisons With Experiment. NACA Rep. 867, 1947. (Supersedes NACA TN 1363.)
4. Steiner, Margaret F.: Comparison of Over-All Impact Loads Obtained During Seaplane Landing Tests With Loads Predicted by Hydrodynamic Theory. NACA TN 1781, 1949.
5. Steiner, Margaret F.: Analysis of Planing Data for Use in Predicting Hydrodynamic Impact Loads. NACA TN 1694, 1948.
6. Lamb, Horace: Hydrodynamics. Sixth ed., Cambridge Univ. Press, 1932.
7. Pabst, Wilhelm: Landing Impact of Seaplanes. NACA TM 624, 1931.
8. Weinstein, Irving, and Kapryan, Walter J.: The High-Speed Planing Characteristics of a Rectangular Flat Plate Over a Wide Range of Trim and Wetted Length. NACA TN 2981, 1953.
9. Chambliss, Derrill B., and Boyd, George M., Jr.: The Planing Characteristics of Two V-Shaped Prismatic Surfaces Having Angles of Dead Rise of 20° and 40°. NACA TN 2876, 1953.
10. Wagner, Herbert: Über Stoss- und Gleitvorgänge an der Oberfläche von Flüssigkeiten. Z. a. M. M., Bd. 12, Heft 4, Aug. 1932, pp. 193–215.
11. Bisplinghoff, R. L., and Doherty, C. S.: A Two-Dimensional Study of the Impact of Wedges on a Water Surface. Contract No. NOa(s)–9921, Dept. Aero. Eng., M.I.T., Mar. 20, 1950.
12. Povitsky, A. S.: The Landing of Seaplanes. Rep. No. 423, Trans. CAHI (Moscow), 1939.
13. Smiley, Robert F.: An Experimental Study of Water-Pressure Distributions During Landings and Planing of a Heavily Loaded Rectangular Flat-Plate Model. NACA TN 2453, 1951.
14. Batterson, Sidney A., and McArver, A. Ethelda: Water Landing Investigation of a Model Having a Heavy Beam Loading and a 30° Angle of Dead Rise. NACA TN 2015, 1950.
15. McArver, A. Ethelda: Water-Landing Investigation of a Model Having Heavy Beam Loadings and 0° Angle of Dead Rise. NACA TN 2330, 1951.
16. Smiley, Robert F.: A Semiempirical Procedure for Computing the Water-Pressure Distribution on Flat and V-Bottom Prismatic Surfaces During Impact or Planing. NACA TN 2583, 1951.
17. Shoemaker, James M.: Tank Tests of Flat and V-Bottom Planing Surfaces. NACA TN 509, 1934.
18. Sottorf, W.: Experiments With Planing Surfaces. NACA TM 661, 1932.
19. Sambraus, A.: Planing-Surface Tests at Large Froude Numbers—Airfoil Comparison. NACA TM 848, 1938.
20. Hedrick, I. G., and Siebert, E. G.: Water Loads Investigation—Airplane Model XJR2F–1. Rep. No. 2903.41, Grumman Aircraft Eng. Corp., May 19, 1946.